Assessments of the WRF model in simulating 2021 extreme rainfall episode in Malaysia.

CHEN, Y., CHAN, A., OOI, C.G., LI, L. and TEA, F.Y.

2024

Assessments of the WRF model in simulating 2021 extreme rainfall episode in Malaysia

Yixiao Chen[1] Andy Chan[2] Chei Gee Ooi[3] Li Li[4] Fang Yenn Teo[1]

1 Faculty of Science of Engineering, University of Nottingham Malaysia, Jalan Broga, 43500 Semenyih, Selangor Darul Ehsan, Malaysia

2 School of Engineering, Robert Gordon University, AB10 7GJ Aberdeen, UK

3 Insitute of Climate Change, Universiti Kebangsaan Malaysia, Bangi, Selangor Darul Ehsan 43600, Malaysia

4 School of Environmental and Chemical Engineering, Shanghai University, 200444 Shanghai, China

Abstract

An episode of extreme monsoonal flood event has severely affected the East and West coast of Peninsular Malaysia from 16th to 18th December 2021. The extreme rainfall was documented to be associated to Tropical Depression 29 and Typhoon Rai. In addition, biomass burning aerosols were suspected to be capable of intensifying the precipitation. Thus, the main causes of this extreme event are studied with model evaluation being carried out with biomass burning as one of the possible reasons and variables. From the sensitivity analysis on the PBL scheme for the model physics, QNSE scheme is tested to be the best scheme to simulate the episode compared with MYJ and ACM2 and used in the model assessment. The performances of ARW (WRF-ARW), BB (WRF-Chem with biomass burning), and NOBB (WRF-Chem without biomass burning) have been assessed in the reproduction of the precipitation pattern and tropical depression. Simulation results indicate that ARW shows an overall better performance for most meteorological variables with better performance in reproducing the surface-level pressure and wind speed. Model scenarios of ARW and BB produced similar tropical depression spatial distributions but differ in magnitude, where the tropical depression in ARW is stronger during the study period over East coastline. All models overestimate the precipitation intensity, but ARW is much better correlated with observation data followed by NOBB and BB. The findings show that biomass burning aerosols have only a minor impact on intensifying or delaying the rainfall event. Therefore, tropical depression over Peninsular Malaysia is shown to be the main causation to this extreme event in 2021. The model could be applied for the future flood risk management in Malaysia to provide information on decision making.

Keywords WRF model; Extreme rainfall; Flooding; Biomass burning; Tropical depression; Peninsular Malaysia

Introduction

Flooding events occur annually during the Northeast monsoon season (NEM) with massive casualties and property losses, especially over the East coast of Peninsular Malaysia(PM), and generally they are mainly categorised as monsoonal flood (Caddis et al. 2012; Sani et al. 2014; Xia et al. 2016; Cheah et al. 2019; Chong et al. 2021; Fung et al. 2022; Tan et al. 2022). Tsay et al. (2013) shows that the precipitation over PM, 1951 to 2012, are related to heavy rainfall cyclone that caused by the cold surge vortices covering two third of the total precipitation amount, and the precipitation was also affected by phenomena such as El Niño Southern Oscillation (ENSO) during the boreal winter (Tsay et al. 2013). Similar result is also found by Lim et al. (2017) that interaction between monsoonal cold surge and Madden–Julian oscillation (MJO) can have a large impact on the rainfall response over Southeast Asia (SEA) (Lim et al. 2017).

In mid-December 2021, an episode of extreme rainfall resulted in destructive floods over PM with 48 casualties, more than 70,000 homeless people and economic losses up to USD $1.46 billion. The unusual situation to this flooding was that it not only affected the East coast but also the West coast of PM where it was normally under the drier conditions from previous NEM, whilst the extra amount of precipitation could be

attributed to tropical cyclonic circulation (Tew et al. 2022). Tropical cyclone (TC)-related precipitations could be classified into direct effect and indirect effect where the former mainly produce heavy rainfall directly by themselves, and the latter one could lead to heavy rainfall in remote area by interacting with other synoptic systems (such as monsoon circulation, topographic effect, cold frontal system) far away from the TC centre (Bosart and Carr 1978; Wang et al. 2009; Chen and Wu 2016; Lin and Wu 2021). The remote rainfall induced by the indirect effect has been observed by several studies. Study from Bosart and Carr (1978) find Hurricane Agnes intensifies the rainfall by transferring moisture from the Western Atlantic to the rainfall region through its outer circulation (Bosart and Carr 1978). Similar results had been indicated by Wang et al. (2009) and Chen and Wu (2016) where the remote precipitation event is strengthened by the typhoons in Japan and Taiwan (Wang et al. 2009; Chen and Wu 2016). The extreme event in PM can be considered as the direct effect from the Tropical Depression 29 (TD) over PM and the remote interaction between Typhoon Rai over the Philippines which transports more moisture to the rainfall region through its outer circulation over this period of time. However, the actual mechanism of the origin of this rainfall episode remains in debate as some research also point to climate change or other weather event as the main cause to this extreme rainfall (Rahman 2022).

Biomass burning (BB) haze is an important anthropogenic aerosol emission sources over SEA which appears almost regularly for the past decades and attracts global and public attentions due to its impact on the visibility, regional climate system, long-range transportation, and human health (Ahmed et al. 2016). BB aerosols plays an important role in altering global and regional climate pattern by affecting radiation budget (Zhao et al. 2020; Jangid et al. 2021) and cloud formation process (Twomey 1997) through aerosol–radiation interaction (ARI) and aerosol–cloud interaction (ACI). ARI is known as the interaction between aerosol and radiation, where earth energy balance is impacted by aerosol through scattering and absorbing solar radiation (Schwartz 1996; Forster et al. 2007; Myhre et al. 2013). Carbonaceous aerosols, such as black carbon (BC) absorb radiation effectively, which warm up the atmosphere and reduce surface radiation, hence lead to surface cooling (Bollasina et al. 2011). It further reduces land–ocean thermal contrast and weakens monsoon circulation (Li et al. 2016). Fan et al. (2009) indicates that ARI tends to reduce surface wind, thereby enhance wind shear and result in inhibiting convection (Fan et al. 2009). From the analyses of observation data in China, it is found that a decrease of 8% of the surface wind under the influence of aerosol radiative effect (Jacobson and Kaufman 2006).

The interaction between aerosol and cloud is known as ACI, where aerosol acts as cloud condensation nuclei (CCN), thereby affecting the albedo and lifetime of cloud and precipitation (IPCC 2014; Wu et al. 2015; Ajoku et al. 2019). ACI primarily refers to the increasing number of cloud droplet due to the increasing concentration of suspended aerosol particles, therefore reducing the radiation from reaching surface (Twomey 1997). Cloud releases more latent heat at higher atmosphere, enhances the convection, cloud development and precipitation, and results a delayed rainfall with stronger intensity (Andreae et al. 2004; Koren et al. 2008; Rosenfeld et al. 2008). Therefore, the effect of BB aerosols on the extreme monsoonal rainfall event is considered important in precipitation generation and is taken into consideration in this study.

Numerical models are widely used to study and understand the mechanism of metrological systems. The Advanced Research online–coupled regional Weather Research and Forecasting model (WRF-ARW) had been examined by several studies on its ability in simulating and forecasting regional climate, which also includes extreme rainfall activity (Chen et al. 2017; Moya-Álvarez et al. 2018; Chang et al. 2019). It has the capability of adjusting physical conditions such as microphysics, cumulus parameterisations, planetary boundary layer physics, and atmospheric radiation physics. The aerosol and trace gas concentration are defined as important components which affect the radiation response within the atmosphere and is fixed in WRF-ARW. While WRF with chemistry (WRF-Chem) model provides adjusting option on producing the forecast by applying real chemistry boundary condition with predicted aerosol and trace gas concentration, compared to WRF-ARW that simulates meteorological processes only, WRF-Chem simulates additional processes such as gas and aqueous phase chemsitry, aerosol microphysics, and feedback mechanisms of gases and aerosols to clouds, radiation, and other meteorological variables and processes (Yahya et al. 2017). Therefore, WRF-CHEM is more used in simulating regional air quality model, as well as in figuring out the effect of BB event by including and excluding the BB emission inventory into the model input (Aouizerats et al. 2015; Oozeer et al. 2016; Zhou et al. 2018; Lee et al. 2018; Liu et al. 2021).

Many studies have conducted sensitivity studies to different meteorological physical parameterisation schemes for both WRF-ARW and WRF-Chem (Crippa et al. 2017; Pegahfar et al. 2022). However, rarely have studies discussed the performance between WRF-ARW and WRF-Chem, as WRF-Chem is always considered to be more accurate than WRF-ARW with better chemical substances concentration. Yahya et al. (2016) compares the simulation result from WRF-ARW and WRF-Chem over America, where WRF-Chem shown better performance in reproducing meteorological elements (temperature, relative humidity, wind speed) as it has more accurate radiation variables. However, precipitations from two models are both overestimated and seem to have no close relationship with aerosol and gas concentration but more relate to model microphysics or convective parameterisations (Yahya et al. 2017). The comparison between the two algorithms is an area we want to insert an effort into. We would also like to understand better the physical mechanism of the cause of the intense precipitation during the period, especially the effect from BB.

Our study aims to evaluate the model performance between WRF-ARW and WRF-Chem in simulating the extreme rainfall event over PM from 15th to 18th December 2021. A sensitivity analysis on the planetary-boundary-layer scheme (QNSE, MYJ, ACM2) is conducted to figure out the best scheme and use for all physical model configuration. Moreover, the effect of BB aerosol on the monsoon-induced low-pressure system over Malaysia is examined through local precipitation, wind pattern, and sea level pressure (SLP). The simulation design and observational dataset are presented. Model performance evaluation and the impact of BB aerosols on the monsoon-driven circulation system over PM are discussed in detail.

Methodology

Observation

The tracks of Typhoon Rai over Indonesia and Tropical Depression 29 (TD) over Malaysia are obtained from International Best Track Archive for Climate Stewardship (IBTrACS) project under National Center for Environmental Information (NCEI). IBTrACS collates TC storm track dataset from global agencies such as World Metrological Organization (WMO), National Hurricane Center (NHC), and Joint Typhoon Warning Center (JTWC).

The observational daily accumulated precipitation data used to identify the spatial and temporary heavy rainfall distribution are obtained from global precipitation measure (GPM) with resolution of 0.1° × 0.1° covering the region over tropical and subtropical ocean. The data are developed from the tropical rainfall measuring mission (TRMM) system which is sensitive to the heavy and moderate precipitation, while GPM is more focused on the light precipitation which can be considered as one of the finest and most accurate satellite precipitation products over tropical areas (Tew et al. 2022). Tan and Santo (2018) shows the smallest uncertainty for the flood 2014–2015 simulations in Malaysia compared to other products (Tan and Santo 2018).

To detect the location of TD, meteorological data such as wind field and sea level pressure (SLP) are obtained in the hourly time-averaged form from the second Modern-Era Retrospective analysis for Research and Applications (MERRA-2) under NASA atmospheric reanalysis for spatial plot (GMAO 2015). 2-metre temperatures (2-m T) are taken from MERRA-2 as well for model evaluation. Observation data used to carry out the statistical analysis are obtained from National Center for Atmospheric Research (NCAR) APD Surface Observational Weather Data (NOAA 2004). The verifications of MERRA-2's meteorological data with observation data are also conducted as shown in Table 5, with correlation coefficient r of 0.68, 0.79, 0.39, and RMSE of 1.86, 1.88, 4.47 for 2-m T, SLP, and wind speed respectively. Although it has slightly overpredicted the surface wind speed, the values for 2-m T and SLP could be considered reliable.

Model settings

The experiments are based on the extreme precipitation event that occurred over PM from 15th to 18th December 2021 and are simulated using WRF-ARW and WRF-Chem (version 3.9.1) with the same model set up for domain and physical parameters (Grell et al. 2005). The study period is from UCT00 on 14th Dec 2021 to at UCT00 on 19th Dec 2021 with 2 days of spin-up for WRF-ARW and 10 days of spin-up for WRF-Chem as the period for model to reach its steady state is different for models include/exclude chemistry reaction. The model domain is shown as Fig. 1 with horizontal resolution of 30 km for the outer parent domain (d01) and horizontal reso-lution of 10 km for the nest domain (d02). It consists of a grid point size with 110×100 and 100×103 for the parent and nest domain respectively, and vertical layer of 35 for both domains. The parent domain includes Sumatra, Kalimantan, Malaysia, and part of Indian Ocean and South China Sea, while the nest domain covers Northwestern Sumatra and PM. The lateral boundary condition updated in 6-h simulation interval and running with four-dimensional data assimilation (FDDA) grid nudging with a 3-h interval. The WRF model output is written every hour.

The meteorological initial and boundary conditions are taken from National Centers for Environmental Prediction FiNaL reanalysis (NCEP-FNL) data with spatial resolution of 1° × 1° and time interval of 6 h. The chemical initial and boundary conditions are MOZART-4 (Model for Ozone and Related Chemical Tracers, version 4) results from the National Center for Atmospheric Research (NCAR). Biogenic emissions are taken from the Emission of Gases and Aerosol from Nature version 2.1 (MEGAN 2.1) (Guenther 2006). Anthropogenic emission of aerosol and trace gas are taken from EDGAR v5.0 Global Air Pollutant Emis-sions (Crippa et al. 2021). The daily open BB emissions are obtained from the Fire iNventory from NCAR (FINNv2), which is derived from the MODIS satellite date of active fire spots, land surface, fuel loading, and emission factors (Wiedinmyer et al. 2011; Zhou et al. 2018). It may therefore lead to over or under-estimation of BB emission due to uncertainties in identifying the classification of fire and land surface, fuel consumption, and emission factors. It is most likely to underestimate the aerosol concentration near surface as satellites are not capable to capture all the smoldering burnings (Lee and Wang 2020). It classifies the burning of extra tropical forest, tropical forest (including peatland), savanna, and grassland, with various of emitted species from biomass burning including organ carbon, black carbon, carbon monoxide, nitrogen oxides, ammonia, and sulphate dioxide. Model initial and boundary condition and emission inventory are listed as Table 1.
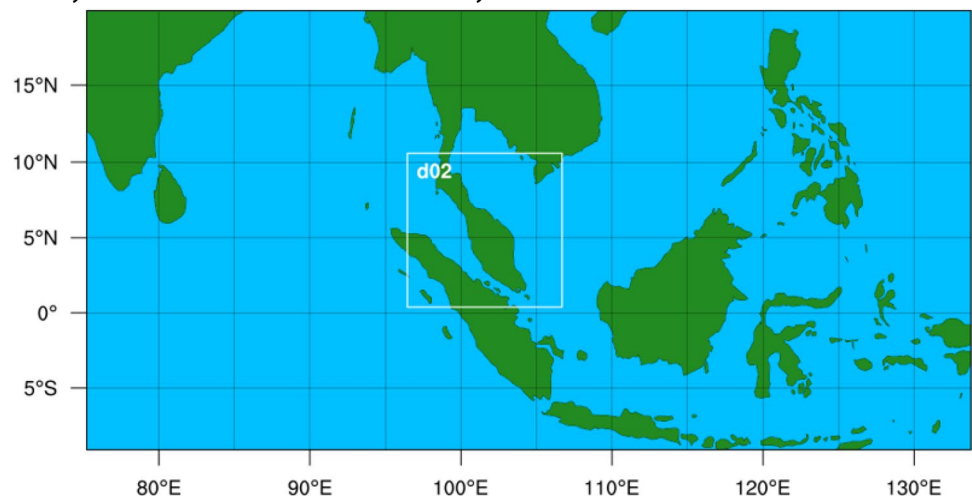
Fig. 1 Model domain

Table 1 Model boundary condition and emission inventory

	ARW	BB	NOBB
Boundary condition			
Meteorological initial and boundary condition	NCEP-FNL	NCEP-FNL	NCEP-FNL
Chemical initial and boundary conditions	-	MOZART-4	MOZART-4
Emission inventory			
Biogenic emission	-	MEGAN 2.1	MEGAN 2.1
Anthropogenic emission	-	EDGAR v5	EDGAR v5
Biomass burning emission	-	FINN v2	-

Table 2 shows the physics and chemistry parameter schemes used in this study. The Morrison 2-moment micro-physics scheme (Morrison) is chosen as the microphysics scheme which is able to estimate the number concentration and mixing ratio of graupel, rain droplet, snow, cloud droplet, and ice particles for physical mechanism of cloud (Oozeer et al. 2016). The rapid radiative transfer model for GCMs (RRTMG) is used in both longwave and shortwave radiation schemes for conducting aerosol–radiation interaction. The NOAH-multi parameterisation land surface model which contains multiple interactions between land and atmosphere, with an aim of proper transfer processes in surface water and energy, is used for land surface model (Tomasi et al. 2017). Cumulus scheme of Grell-3 developed from Grell–Devenyi (GD) cumulus scheme, which allows cloud radiation and aerosol–cloud interaction to receive more feedback from convection process. As for chemistry scheme, MOZART and Model for Simulating Aerosol Interactions and Chemistry (MOSAIC) are selected for gas phase and aerosol mechanism respectively. The aerosol direct effect is turned on by activating aerosol radiative feed-back in the model. The scheme of Madronich F-TUV was used for the photolysis scheme. MOSAIC with volatility basis set (VBS) has been widely used due to its easy coupling between various chemical and microphysical processes. Important types of aerosols are included in the MOSAIC scheme after specifying all the major aerosols from the scale of urban, regional, and global, such as sulfate, nitrate, chloride, carbonate, black carbon, organic carbon, liquid water, and other inorganic aerosols (Zaveri et al. 2008). Table 3 explains the three planetary-boundary-layer (PBL) schemes selected for the sensitivity analysis in this study: Quasi-Normal Scale Elimina-tion (QNSE), Mellor-Yamada-Janjić (MYJ), and Asymmetric Convective Model v2 (ACM2), while other physics parameterisation schemes keep unchanged.

Table 2 Model physics and chemistry

Model physics (ARW, BB and NOBB)	
Microphysics scheme	Morrison 2-moment
Longwave radiation scheme	RRTMG
Shortwave radiation scheme Land	RRTMG
surface model scheme	Noah-MP land-surface model (NOAH)
Cumulus scheme	Grell-3
Planetary boundary layer scheme	Shown as
Model Chemistry (BB and NOBB)	Table 3
Gas phase mechanism	MOZART
Aerosol mechanism	MOSAIC with VBS

Sensitivity analysis between three PBL schemes conducted first to examine the best physics scheme model setup for this rainfall event in Malaysia, and used in the following section. Evaluation between ARW (model without chemistry) and BB (chemistry including BB emission) are used to figure out the most suitable WRF simulation mode (WRF-ARW or WRF-Chem) in reproducing the rainfall event. The impact of BB aerosols can be investigated by comparison between BB and NOBB (model with chemistry excluding BB emission).

Table 3 Model physics for WRF-ARW sensitivity experiments

Simulations	Microphysics	LW/SW radiation	Cumulus scheme	PBL	Surface layer
SIM1	Morrison 2-moment	RRTMG	Grell-3	QNSE	QNSE
SIM2				ACM2	Monin-Obukhov
SIM3				MYJ	Eta model

WRF-ARW sensitivity analysis with PBL scheme

PBL as the lowest atmospheric layer which is highly affected by the exchange of momentum, heat and water from earth surface (Avolio et al. 2017). Its thermodynamic structure plays an important role in reducing the uncertainty for mesoscale model forecasting (Valappil et al. 2023). PBL schemes in WRF model can be classified based on the closure types (local and non-local) depending on the extent to which the known variables can impact a specific model point (Stensrud 2007) and turbulent orders (1.0, 1.5, 2.0). The variables at a specific point in the local closure scheme are only influenced by the immediately adjacent vertical levels, and the PBL height (PBLH) is calculated by using Richardson bulk number method. As for non-local closure scheme, variables can be affected from other vertical levels, and the PBLH is determined at the level where turbulent kinetic energy (TKE) decrease to certain threshold value.

Two local (MYJ, QNSE) and one non-local (ACM2) PBL schemes are selected for this research. MYJ is a 1.5-order prognostic turbulent kinetic energy (TKE) scheme with local vertical mixing (Janjic 2002), and modified from the eta operational scheme (Janjić 1990). The PBLH is determined by TKE decreased to the value of 0.2 m2 s−2. QNSE is a local 1.5-order prognostic TKE scheme with consideration of wave phenomena within stable boundary layers (Sukoriansky et al. 2005). The PBLH is determined by TKE decreased to the value of 0.01 m2 s−2 (Valappil et al. 2023). The PBLH is determined with threshold Richardson bulk number between 0 to 0.25. ACM2 is a 1-order scheme which modified form the ACM1 scheme (Pleim 2007) with combination of local downward mixing and non-local upward mixing approaches. The PBLH is determined at the level where surface Richardson bulk number exceeds 0.25.

Model evaluation

The focus of the model evaluation was to evaluate the climatological model performance under the three model setups to analyse the ability of model on reproducing the monsoonal precipitation and meteorological environment which includes surface level pressure (SLP), 2-m T, and wind speed. The main statistics used for model evaluation are correlation coefficient (r), root mean square error (RMSE), index of agreement (IOA), and normalized mean bias (NMB).

Meteorological variables are evaluated with 6-h NCAR APD Surface Observational Weather Data with 11 stations that spread evenly over PM as shown as Fig. 2. While daily precipitation from model is evaluated with GPM, for this comparison, the grid index corresponding to the geographic location of each station is first determined. The model value of the required variables at the estimated grid index is then calculated by bilinear interpolation from the surrounding four model grid points. The observations and simulations are paired up according to the time and site location, and then averaged to obtain daily observation and simulation data pairs at each site. The statistics are calculated based on the observation and simulation paired averaged data at different sites to provide evaluation,

$$r = \frac{1}{n-1} \sum_{i=1}^{n} \frac{\left(O_i - \underset{-}{O}\right) \times \left(M_i - \underset{-}{M}\right)}{\sigma_o \times \sigma_m} \tag{1}$$

$$RMSE = \sqrt{\frac{\sum_{i=1}^{n} \left(O_i - M_i\right)^2}{n}} \tag{2}$$

$$IOA = 1 - \frac{\sum_{i=1}^{n} \left(O_i - M_i\right)^2}{\sum_{i=1}^{n} \left(\left|M_i - O_i\right| + \left|O_i - O_i\right|\right)^2} \tag{3}$$

$$NMB = \frac{\sum_{i=1}^{n} \left(M_i - O_i\right)}{\sum_{i=1}^{n} O_i} \tag{4}$$

where O represents the observational value, M the values from the WRF simulation, n the number of data, and σ is standard deviation.
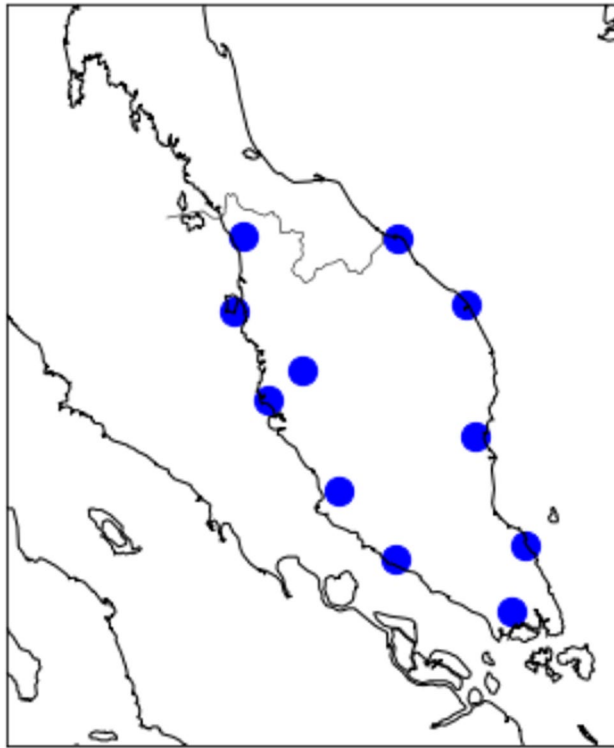
Fig. 2 Spatial distribution of the surface station

Result and discussion

Extreme rainfall event

The Northwest winter monsoon season in SEA usually occurs from November to March, and the prevailing surface wind blows from the Northwest over the MC towards the Intertropical Convergence Zone (ITCZ) that is located between 5°S and 15°S. Tropical cyclone (TC) is known to have a tight association with the monsoon due to its favourable environment for TC formation (Chang et al. 2004). More than 75% of identified tropical storms forming in the monsoon environment (Loo et al. 2015). Chang and Tsay et al. (2013) indicate the contribution of heavy rainfall/flood cyclone event to total rainfall in Malaysia was up to 66% (Tsay et al. 2013). Heavy rainfall event in PM during study period is mainly a result of monsoon-driven TC activity.

Figure 3 shows the tracks of Typhoon Rai over Indonesia and TD over Malaysia. The tropical storm formed over the Western Pacific Ocean on 12th December 2021 and moved Northwestward. It developed into a typhoon with maximum sustained wind speed between 59 to 69 m s−1 when it approached the Philippines on 1800 UCT 15th December. After landfall was made on Siargao Island in Southeastern Philippines on 0900 UCT 16th December, it continued travelling Northwestward to South China Sea with heavy rainfall and sustained wind speed between 49 to 70 m s−1, and finally downgraded to a TD after 1200 UCT 20th December near Hainan. While TD was formed on 1800 UCT 16 December at East coast of PM, it spreaded across PM and weakened at West coast of PM with maximum wind speed of 20 m s−1. Figure 4 shows the 10-m wind field, SLP, and precipitation over PM and SCS from 15th to 18th December 2021, where the first two variables are obtained from MARRA-2 and the latter one obtained from GPM. The TD was initiated over SCS on 15th December, gradually moved West wards towards PM and strengthened by the adequate moisture that supplied by the stronger low-level Northeasterly wind from SCS to the PM. The TD-induced rainfall was firstly concentrated over the East coast (states of Pahang and Terengganu) up to 200 mm/day on 16th December, growing even stronger on 17th and 18th December 2021 with extreme rainfall of 350 mm/day over the West coast (states of Selangor and Perak). It also matched the average precipitation pattern from surface stations as shown in Fig. 5 where East coast experienced maximum rainfall on 16th December, while West coast experienced maximum rainfall on 17th December.

Fig. 3 Track of Typhoon RAI (right) over Indonesia and Tropical Depression 29 (left) over Malaysia. The dot in the red box covers path between 16th and 18th Dec 2021
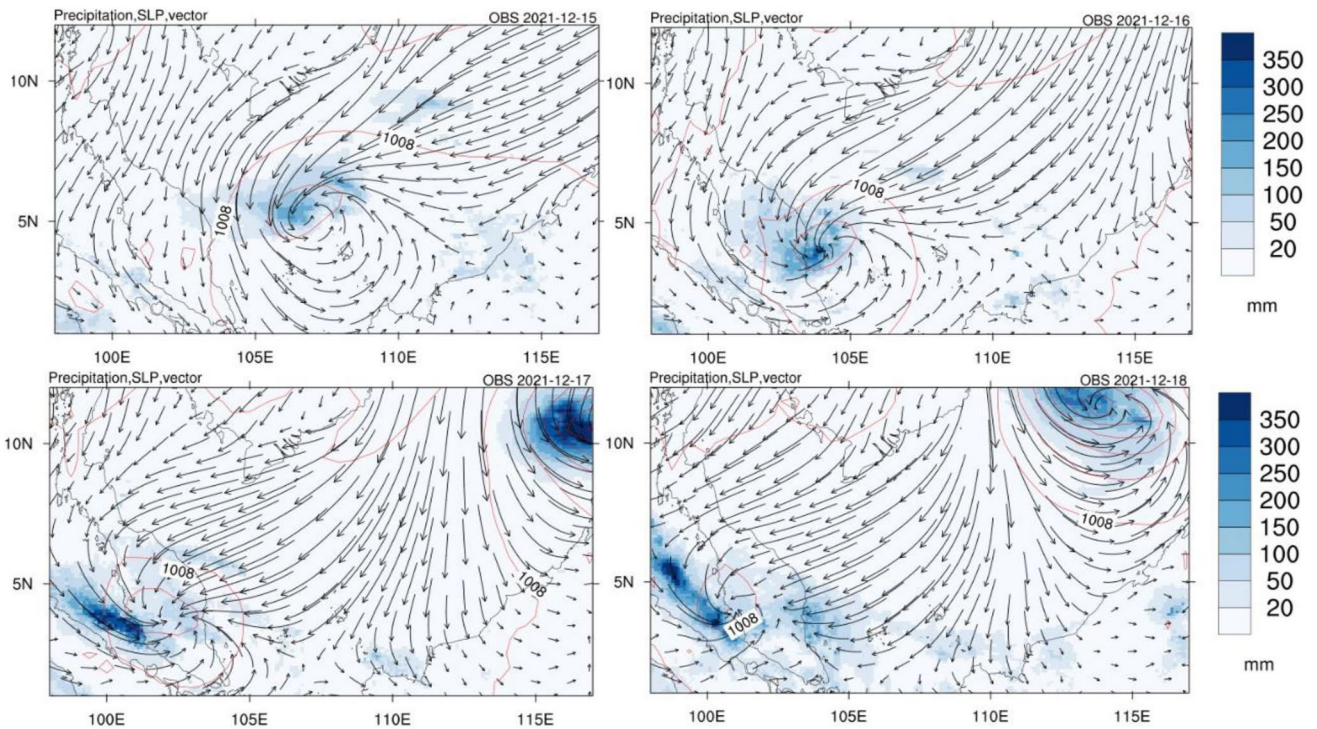

Fig. 4 Daily precipitation (shading, mm), SLP (contours, hPa), and wind field (vector) at 10 m from 0000 UCT 15th December 2021 to 0000 UCT 18th December 2021

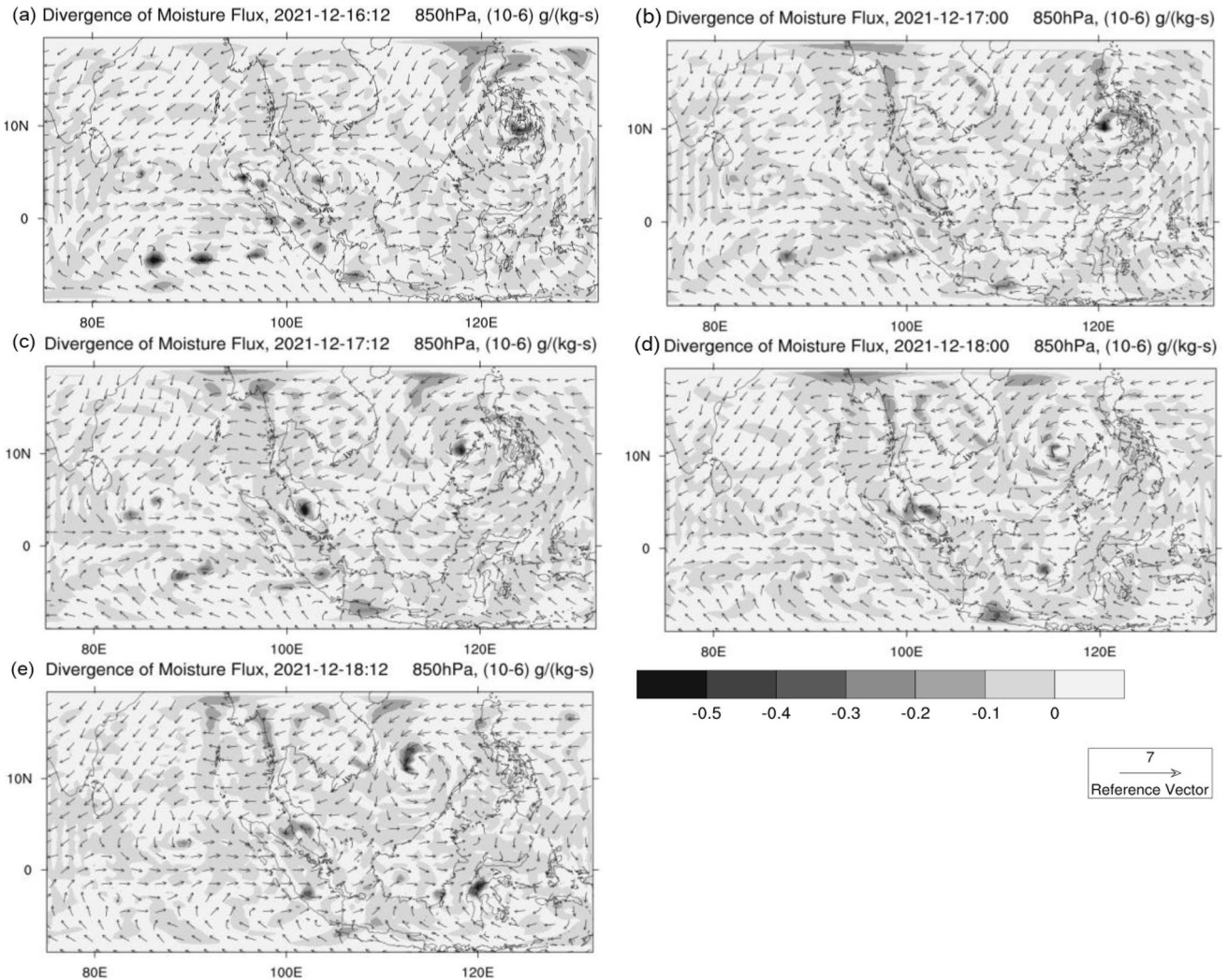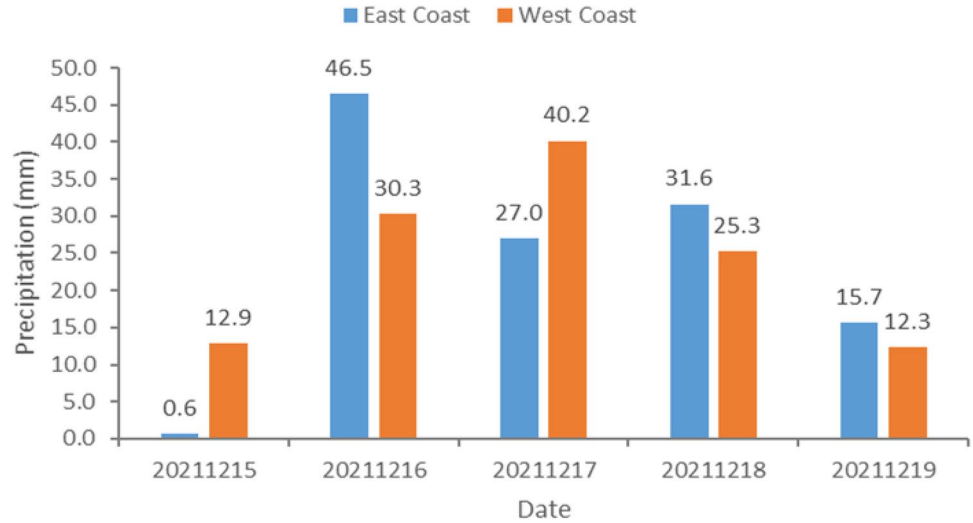**Fig. 5** Average daily station precipitation of east coast and west coast over PM

Fig. 6 Moisture flux divergence (10^{-6} g kg^{-1}s) at 850 hPa at 1200 UCT 16th December (**a**), 0000 UCT 17th December (**b**), 1200 UCT 17th December (**c**), 0000 UCT 18th December (**d**), and 1200 UCT 18th December (**e**) 2021 from MERRA-2

Figure 6 displays the moisture flux divergence at 850 hPa from 1200 UCT (universal coordinated time) 16thDecember to 1200 UCT 18th December in a 12-h interval during the heavy rainfall period form MERRA-2 dataset. The area withlarge moisture convergence is collocated with the regions with heavy rainfall, where East (West) coast experienced heavy rainfall on 1200 UCT 16th December (17th December). The large moisture flux convergence existed in the inner core region of TD with maximum occurring at 1200 UCT 17th December which gathered the moisture from Indian Ocean and SCS. However, the moisture flux convergence between Typhoon Rai and TD is not obvious with most value below 0.1. Therefore, the extreme rainfall event over PM would consider to be mainly caused by direct effect of TD rather than the remote effect from Typhoon Rai as it only had limited contribution in transport moisture to PM during the study period. Moreover, a time lag between the occurrence of biomass burning activity and its impact on rainfall patterns has been observed in the several research, as aerosols take time in transferring to cloud condensation nuclei and affects convective system (Khain et al. 2004; Tao et al. 2007; Chen et al. 2023). Therefore, the impact of the biomass burning aerosol on the rainfall event was also con-sidered in the following sections as burning activities were observed over Southern PM that observed in Fig. 7 on 25th November 2021.
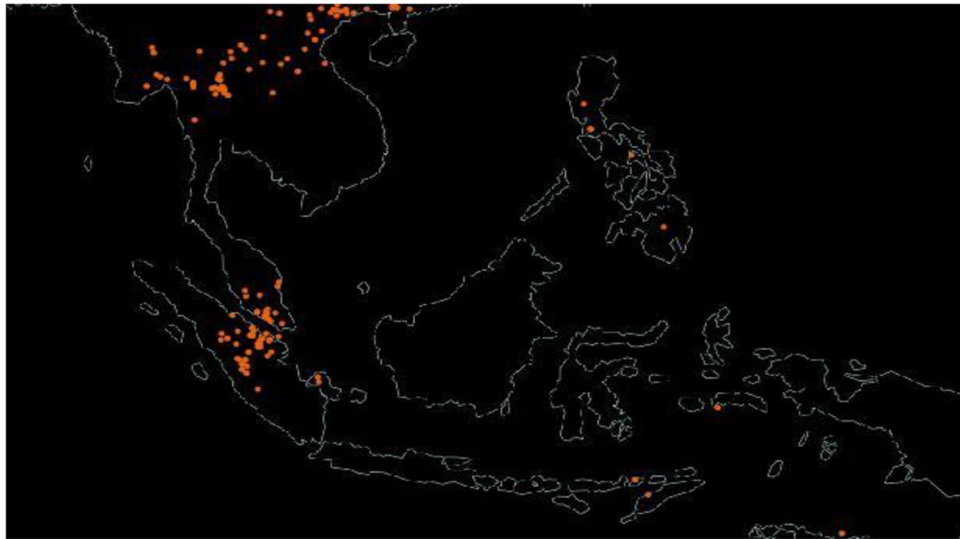

Fig. 7 Thermal anomalies from NASA Worldview server on 25th November 2021

WRF-ARW sensitivity on surface meteorological variables

Figure 8 presents the spatial distribution of accumulated total precipitation produced by WRF-ARW with three PBL schemes against GPM over PM from 0000 UCT 16th December 2021 to 0000 UCT 18th December 2021. In general, the rainfall distributions from three simulations show huge difference points out the important role of PBL plays in affecting the rainfall pattern and characteristics.

The heavy rainfall centre is observed to be located over Southeast (> 150 mm) and Southwest (> 200 mm) coastline over PM as shown in GPM observation. The Southeast heavy rainfall centre simulated by SIM1 scheme tends to have moved to the Northeast PM with similar intensity. Similar shifting is also observed in SIM2, but it moves further North to the Northern PM. SIM3 tends to underestimate the rainfall intensity over Southeast coastline with mostly below 100 mm. As for the rainfall centre over Southwest coast-line, SIM3 has successfully reproduced the pattern along the Strait of Malacca with much lower intensity, and SIM1 performs better in simulating higher magnitude over South-west PM compared to another PBL schemes. As the extreme rainfall is investigated to be resulted from TD, the distribution of SLP is also compared for the analysis as Fig. 9.
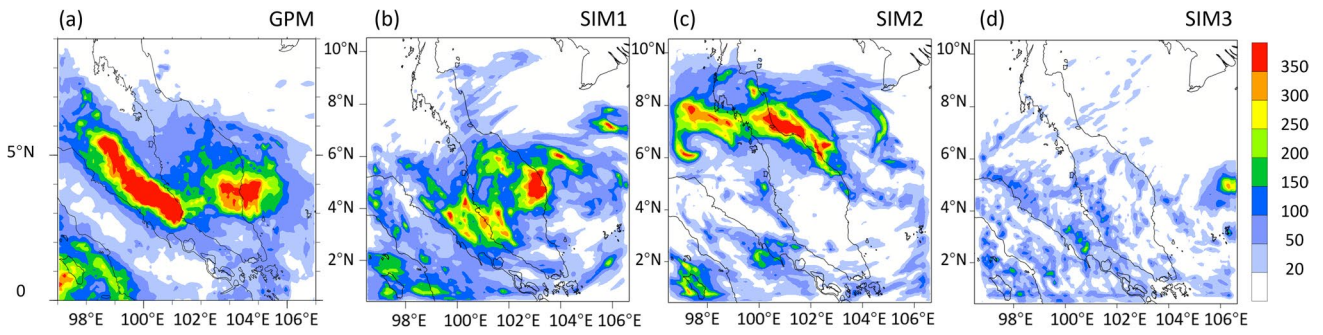
Fig. 8 Accumulated total precipitation (mm) spatial distribution of GPM (**a**) and different PBL schemes (**b**, **c**, **d**) for the period from 0000 UCT 16th December 2021 to 2300 UCT 18th December 2021
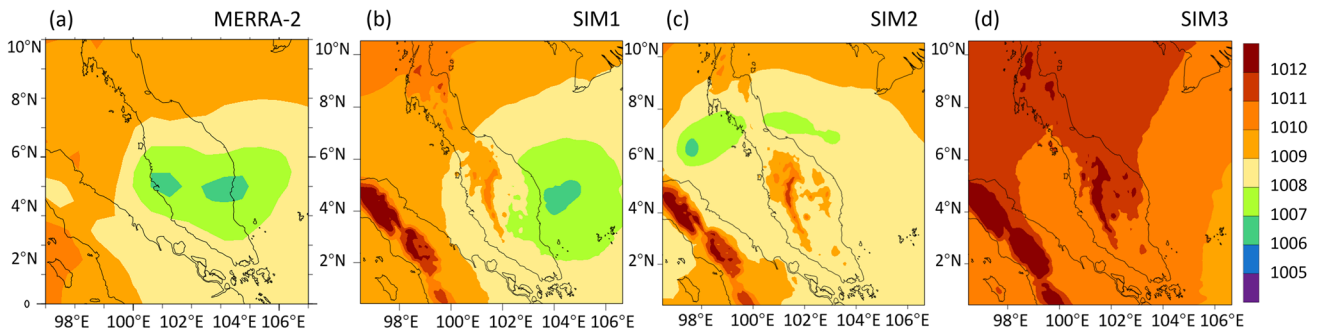

Fig. 9 Average SLP (hPa) of MERRA-2 (**a**) and different PBL schemes (**b**, **c**, **d**) for the period from 0000 UCT 16th December 2021 to 2300 UCT 18th December 2021
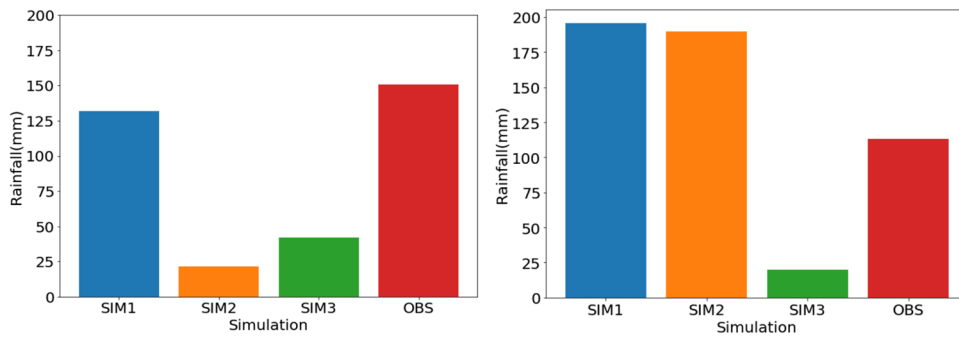

Fig. 10 Averaged WRF-simulated total accumulated precipitation corresponding to different PBL schemes and observations (OBS) for the period from 0000 UCT 16th December 2021 to 2300 UCT 18th December 2021 over western (left) and eastern (right) stations

Table 4 Summary of statistical analysis on meteorological variables for different PBL schemes

	Simulation	RMSE	r	IOA	NMB
Precipitation	SIM1	51.06	0.49	0.41	81%
	SIM2	49.05	0.53	0.41	7%
	SIM3	45.48	0.43	0.34	-34%
2-m temperature	SIM1	1.84	0.72	0.76	-4%
	SIM2	1.93	0.63	0.71	-1%
	SIM3	2.12	0.64	0.72	-2%
2-m wind speed	SIM1	2.59	0.50	0.47	112%
	SIM2	2.01	0.27	0.44	59%
	SIM3	1.95	0.35	0.46	49%
SLP	SIM1	1.43	0.54	0.64	0%
	SIM2	1.61	0.36	0.49	0%
	SIM3	1.96	0.41	0.53	0%

Comparing with the MERRA-2 dataset (Fig. 9a), SIM3 underestimates the strength of the TD, which also includes the weak rainfall intensity observed in Fig. 8. The centre of TD simulated by SIM2 moves to the Strait of Malacca. SIM1 is able to reproduce the TD pattern (location and strength) over East coast; however, the TD is unable to travel across the PM to the West coast. Overall, SIM1 (QNSE) gives the better performance in reproducing the rainfall distribution and intensity, and the strength and location of TD compared to another three simulations.

The total accumulated precipitation of station observation and three simulations averaged over western and Eastern stations is shown as Fig. 10. Over west coastline, SIM1 is the closest to the observation compared to other two simulations where largely underestimate rainfall. As for stations over the East coast, SIM1 and SIM2 have similar performance in overestimating the rainfall intensity with difference of 70 mm com-pared to station data. Table 4 presents the statistical analysis (RMSE, r, IOA, and NMB) of meteorological variables (precipitation, 2-m temperature, 2-m wind speed, and SLP) for different PBL schemes against station observation data, which provides a more direct view on the performance of each simulation experiment. All three simulations show poor correlation in forecasting precipitation and 2-m wind speed, which could be attributed from the high spatiotemporal deflection in simulating tropical depression over PM. The statical parameters of precipitation does not show which PBL scheme performs better in reproducing the extreme rainfall event over PM. However, SIM1 can be considered as best PBL scheme due to its better performance in statistical analysis for other variables.
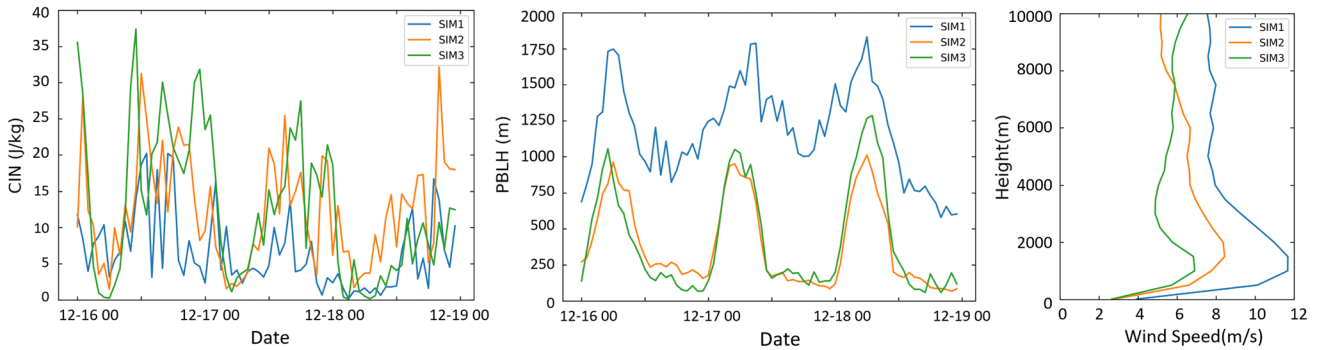

Fig. 11 Time series of station averaged CIN (left) and PBLH (middle) corresponding to different PBL schemes. Station averaged wind speed (right) at different level averaged for the period from 0000 UCT 16th December 2021 to 2300 UCT 18th December 2021

Figure 11 (left) depicts the temporal variation of convective inhibition (CIN), which is used to examine the amount of energy required for an upwardly rising air parcel to reach its free convection state. The lower the value of CIN, the easier for convection to occur. SIM1 (QNSE) keeps the lowest CIN value throughout the precipitation period, creating a favourable environment for precipitation formation (2023 Valappil). Figure 11 (middle) shows the temporal variation in PBL height (PBLH) from 16th to 18th December 2021, with higher values during daytime and lower values during night. SIM1 has deeper PBLH compared to the other two schemes, resulting in a better convective condition with higher moisture instability and moisture transfer during precipitation period (Verma et al. 2021). The vertical variabilities in station-averaged wind speed are shown as Fig. 11 (right). For 3 simulation scenarios, the maximum wind speed occurred at lower atmosphere (below 2 km) under the influence of depression, with highest in SIM1 and followed by SIM2 and SIM3. SIM1 has larger difference in wind speed between neighboring layers indicates strong wind shear at lower atmosphere, which moderates the moisture distribution and increases the PBLH (Rai and Pattnaik 2019). Overall, the results that the reproduction of rainfall intensity and distribution is very sensitive to the PBL scheme during model simulation. QNSE scheme (SIM1) performs the better than ACM2 (SIM2) and MYJ scheme (SIM3). Nevertheless, more improvement can be made in the future on the rainfall event prediction by using other model physical schemes, simulating with higher spatial resolution, and different spin-up time.

Table 5 Summary of mean value and statistics of meteorological variables for observation and models

		Precipitation (mm)	2-m T (°C)	SLP (hPa)	WS (m s^{-1})
Meanvalue	OBS	19.09	26.06	1009.29	2.00
	MERRA-2	-	27.73	1011.01	6.23
	ARW	32.29	25.03	1008.74	3.82
	BB	35.72	25.02	1008.52	4.10
	NOBB	36.74	24.84	1008.64	4.27
r	MERRA-2	-	0.68	0.79	0.39
	ARW	0.49	0.72	0.54	0.50
	BB	0.46	0.72	0.52	0.44
	NOBB	0.50	0.77	0.61	0.44
RMSE	MERRA-2	-	1.86	1.88	4.47
	ARW	51.06	1.84	1.43	2.59
	BB	53.98	1.91	1.58	2.93
	NOBB	56.86	1.94	1.42	3.09
IOA	MERRA-2	-	0.46	0.23	0.56
	ARW	0.41	0.76	0.64	0.47
	BB	0.32	0.75	0.60	0.44
	NOBB	0.33	0.75	0.67	0.44
NMB	MERRA-2	-	6%	0.17%	273%
	ARW	81%	-4%	0%	112%
	BB	122%	-4%	0%	128%
	NOBB	132%	-5%	0%	137%

Evaluation for meteorological predictions

Table 5 summarises the statistics for 2-m T, SLP, wind speed (WS), and precipitation respectively from MERRA-2 and three simulation scenarios throughout the study period. Model overall performance is good for 2-m T with a under-prediction by 1°C compared with MERRA-2 of 1.6°C, and the NMB also falls within the range between

−4 to −5%. The model tends to slightly underestimate SLP, but overestimate wind speed and precipitation compared to observation data with average of 2.1 m s^{-1} and 4.8 mm respectively. Overall, WRF simulation tends to perform better than MERRA-2 with its finer resolution. Amongst the three models, ARW shows good performance in reproducing wind pattern with value of 2.59, 0.5, and 112% for RMSE, IOA, and NMB respectively. BB and NOBB have similar performances in producing 2-m T, while SLP in NOBB performance better than BB by looking at the value of r, RMSE, and IOA. All three scenarios tend to overpredict precipitation. In the overall comparison, no single model shown the best reproduction in four meteorological variables from the information in Table 5. Figure 12 gives a more comprehensive view on the spatial distribution by displacing the day average meteorological variables into Northern (Southern) PM and East (West) Coast. From Fig. 12, models underestimate average 2-m T and SLP for most of the stations, especially over East coast, while MERRA-2 tends to overestimate. As for average precipitation, ARW is observed to be closer to the observation data for most stations than BB and NOBB where they largely overpredict the precipitation over Northern PM (station 1 and station 2). All models including MERRA-2 have overestimated the surface wind speed over PM during the study period.

Figure 13 shows the movement of TD from MERRA-2 and three model scenarios. All simulations successfully estimate the TD landfall time and location over central east coast on 16th December. However, TD from simulations fails to cross over the PM to West coast but stays over Northern East coast on 17th and 18th December which might relate to the model planetary-boundary-layer scheme. MERRA-2 shows a similar TD pathway as Fig. 3 where it lands at Pahang and move westwards and dissipates over Strait of Malacca. Figure 14 shows the spatial distribution of precipitation during the study period from GPM and three model scenarios. These simulations tend to predict the heavy rainfall area more Northly on 16th and 17th December where the rainfall centre simulations are observed at the East and West coast from GPM on the respective days.
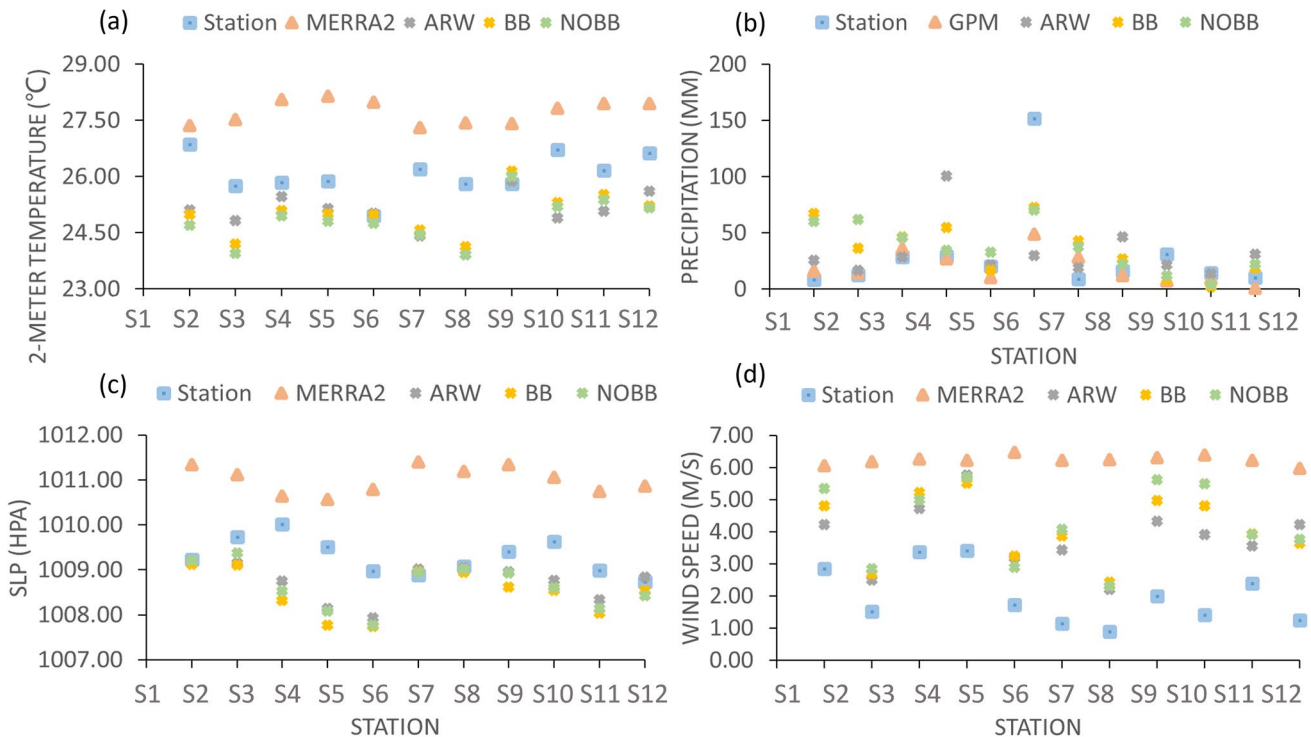

Fig. 12 Average meteorological variables of 2-m T (**a**), precipitation (**b**), SLP (**c**), and wind speed (**d**) from 15th December to 19th December for 11 stations on observation data, MERRA-2, ARW, BB, and NOBB. Station 1 and 2 (10 snd 11) represent Northern PM (Southern PM), and station 3, 4 and 8 (5, 6, 7, and 9) represent East Coast (West Coast)
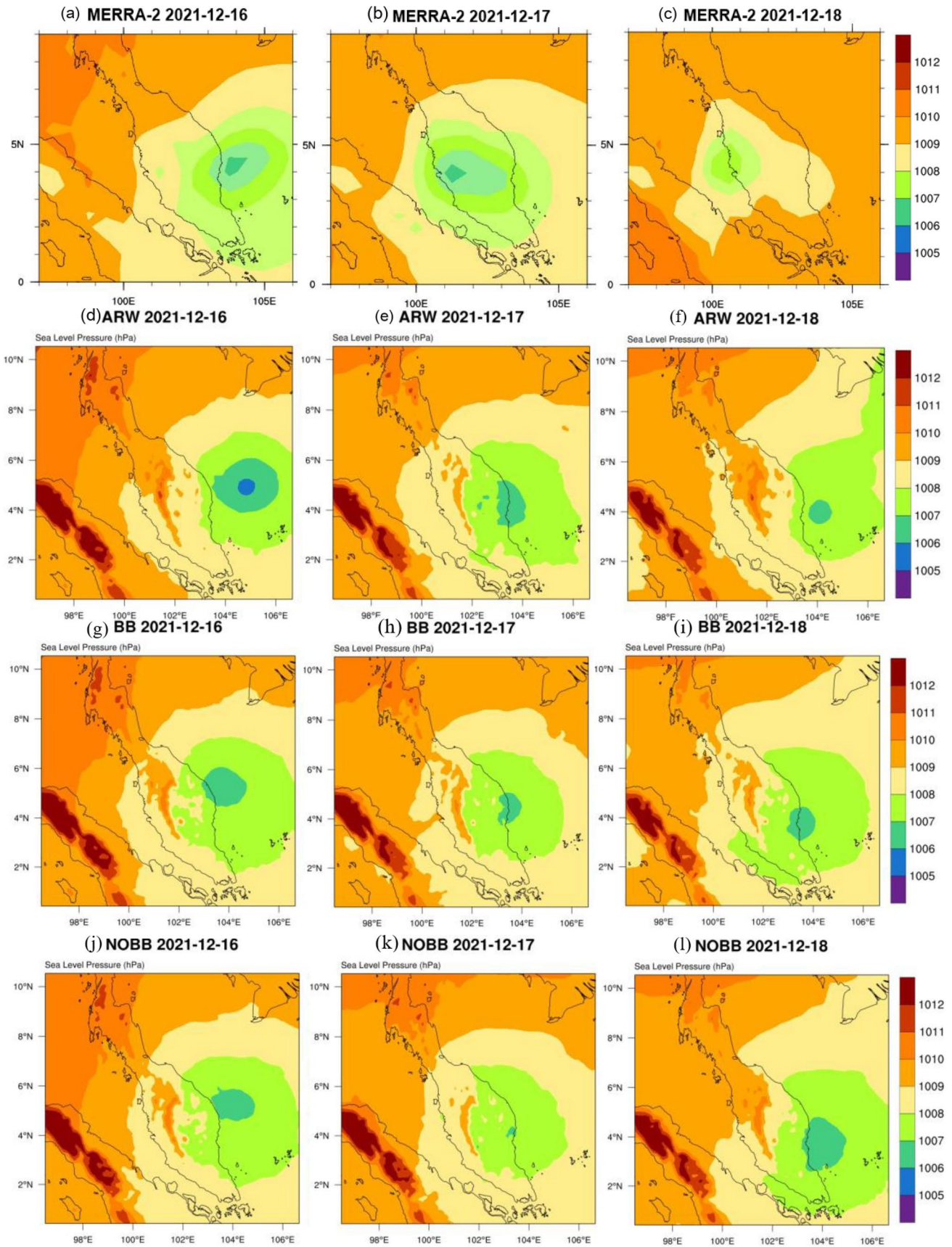
Fig. 13 Spatial distribution of SLP (hPa) from MERRA-2 (**a**, **b**, **c**) against ARW (**d**, **e**, **f**), BB (**g**, **h**, **i**), and NOBB (**j**, **k**, **l**)
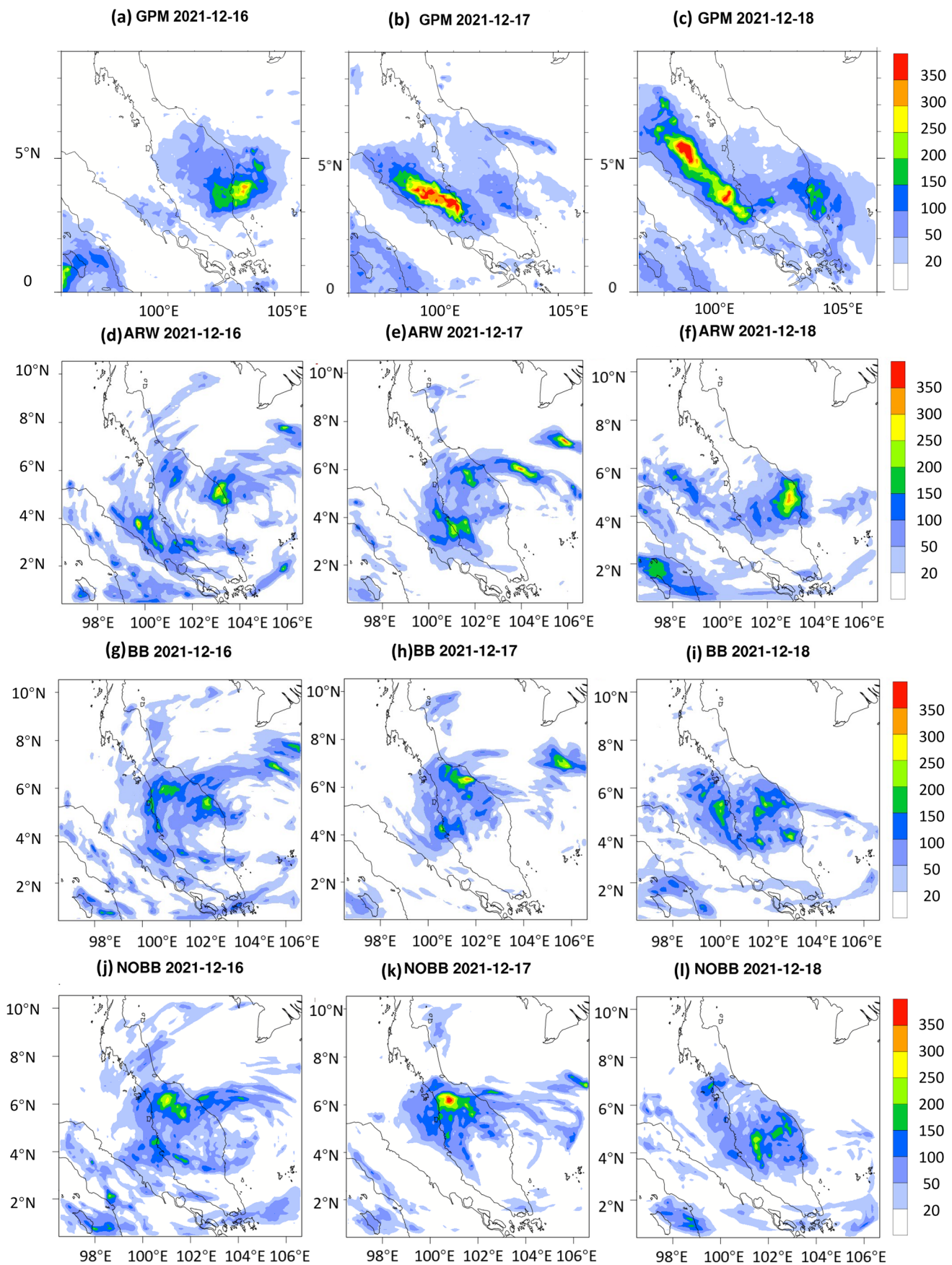
Fig. 14 Spatial distribution of precipitation (mm) from GPM (a, b, c) against ARW (d, e, f), BB (g, h, i), and NOBB (j, k, l)

ARW shows better capability in producing the rainfall distribution over West and East coast on 17th and 18th December, although it overestimates (underestimates) the intensity over East (West) coast. BB and NOBB produce similar performance in the intensity and spatial pattern, while BB performs better on 18th December as the heavy rainfall is produced over Northern West coast but in lower intensity compared to GPM. Figure 15 compares the wind pattern from MERRA-2 and models from 16th to 18th December. BB and NOBB produce similar wind speed pattern on 17th and 18th December with maximum wind speed of 12 m s^{-1} over West and East coast which is consistent with MERRA-2, while ARW has lower wind speed between 5 and 10 m s^{-1} with over the most regions. However, based on the statistics from Table 5, wind speed from MERRA-2 and WRF simulations are all overestimated compared to the station observation, which may attribute to the complexity in topography that cannot be accurately reproduced by coarse resolution (Islam et al. 2018). The spatial distribution of 2-m T is plotted as Fig. 16, where all three models show similar performance and good agreements with MERRA data.

Impact of biomass burning aerosol on the precipitation event

By comparing the concentration of $PM_{2.5}$ between BB and the NOBB-BB (difference between NOBB and BB) in Fig. 17, it is obvious that all the $PM_{2.5}$ comes from the BB inventory; therefore, it is used as an indicator of biomass burning aerosols (BBA). The low concentration of $PM_{2.5}$ (0–0.4 μg m^{-3}) simulated with BBA (Fig. 17 a, b, and c) on the TD's pathway (SCS and PM) indicates that not much BBA is present; therefore, it may have limited influence on the meteorological field during study period. The surface cooling effect from aerosol effect is not observed from this case as BBA is not concentrated enough to initiate the radiation effect.

Figure 18 is used to further verify the impact of BBA by showing the difference of meteorological variables between NOBB and BB during 16th and 18th December 2021. Not much difference in precipitation and wind pattern is observed between NOBB and BB simulation during the study period as the difference is mainly due to the deviation in simulating the TD path. On 18th December, the precipitation intensity over West coast is slightly higher under BB scenario. It also consists with SLP pattern on 18th December as depression over West coast is stronger under the impact of BBA. Figure 19 shows the temporal variation of simulated hourly precipitation over East and West coast. BBA tends have no impact on intensifying or delay the rainfall as the trends form two simulations are similar.

Impact of prognostic and prescribed gas and aerosol concentrations

As the spin-up time applied in the simulation is different between ARW and BB, the distribution of SLP and precipitation on 14th December 2021 of two scenarios are plotted as Fig. 20 to evaluate if it makes a significant contribution to the analysis. The result shows that depression in BB is slightly wider range with SLP between 1007 and 1008 hPa over SCS, but the central location and intensity are not significantly different. The precipitation pattern and intensity almost the same between ARW and BB model simulation. Overall, the discrepancy due to the model spin-up time has little impact on the meteorological field over the study period. Figure 21 shows the difference of meteorological variables between WRF without chemistry (ARW) and WRF with chemistry (BB) during 16th and 18th December 2021. By comparing the SLP difference between two models, ARW simulates stronger depression over East coastline on 16th December which also consistent with the wind circula-tion where the wind speed in ARW is up to 4 m s^{-1} on the same day. The depression simulated by BB on 17th and 18th December tends to be stronger than ARW which accompanied by the strong wind over West coast. As for precipita-tion, ARW (BB) tends to produce heavier over Southern (Northern) PM during study period. From Table 5, both ARW and BB tend to overpredict the precipitation which indicates the precipitation pattern may not largely affected by the aerosol and gas concentration distribution in model but more attributed to the model microphysics or convective parameterisations which is similar to earlier finding (Yahya et al. 2016).
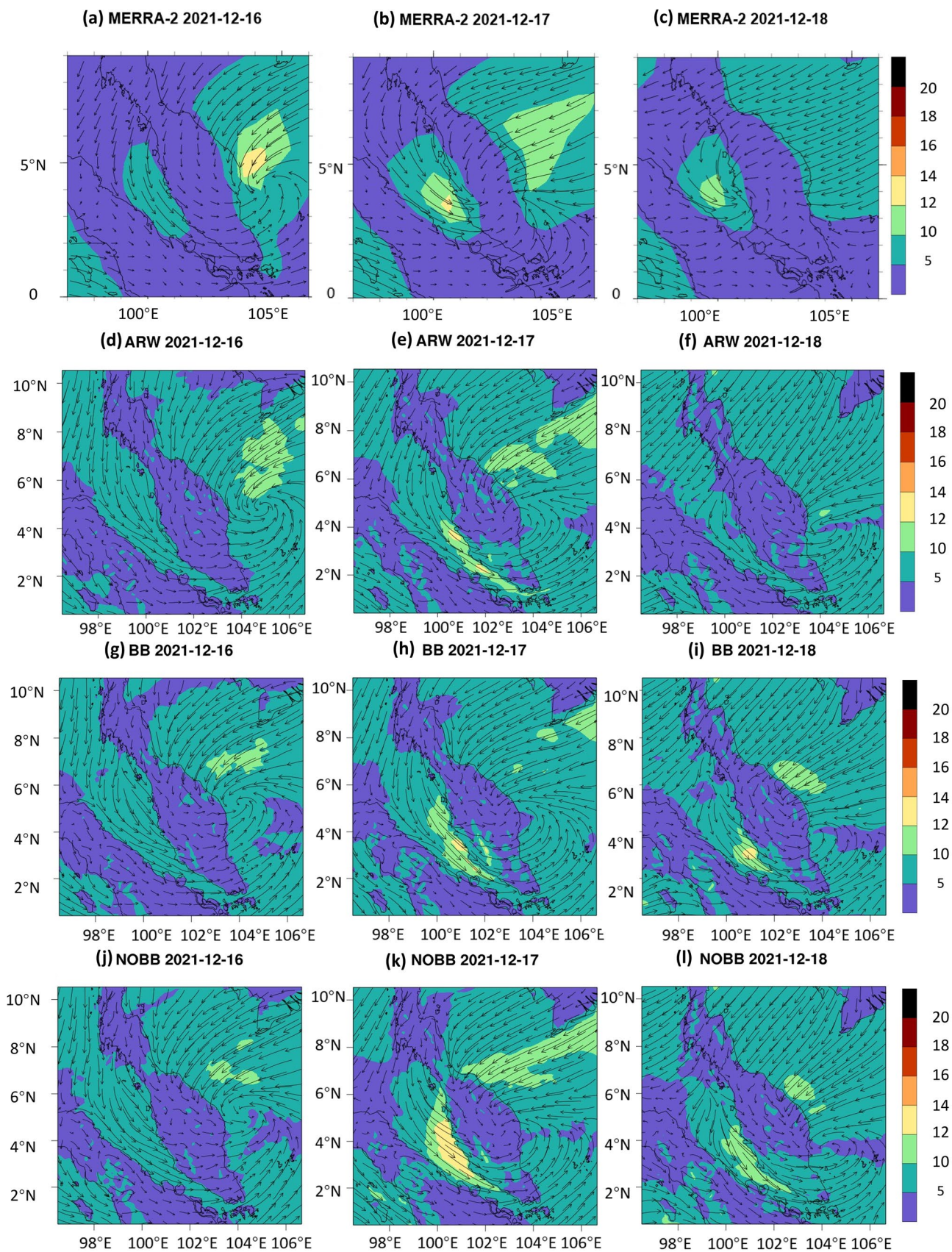
Fig. 15 Spatial distribution of wind speed (m s^{-1}) and field from MERRA-2 (**a**, **b**, **c**) against ARW (**d**, **e**, **f**), BB (**g**, **h**, **i**), and NOBB (**j**, **k**, **l**)
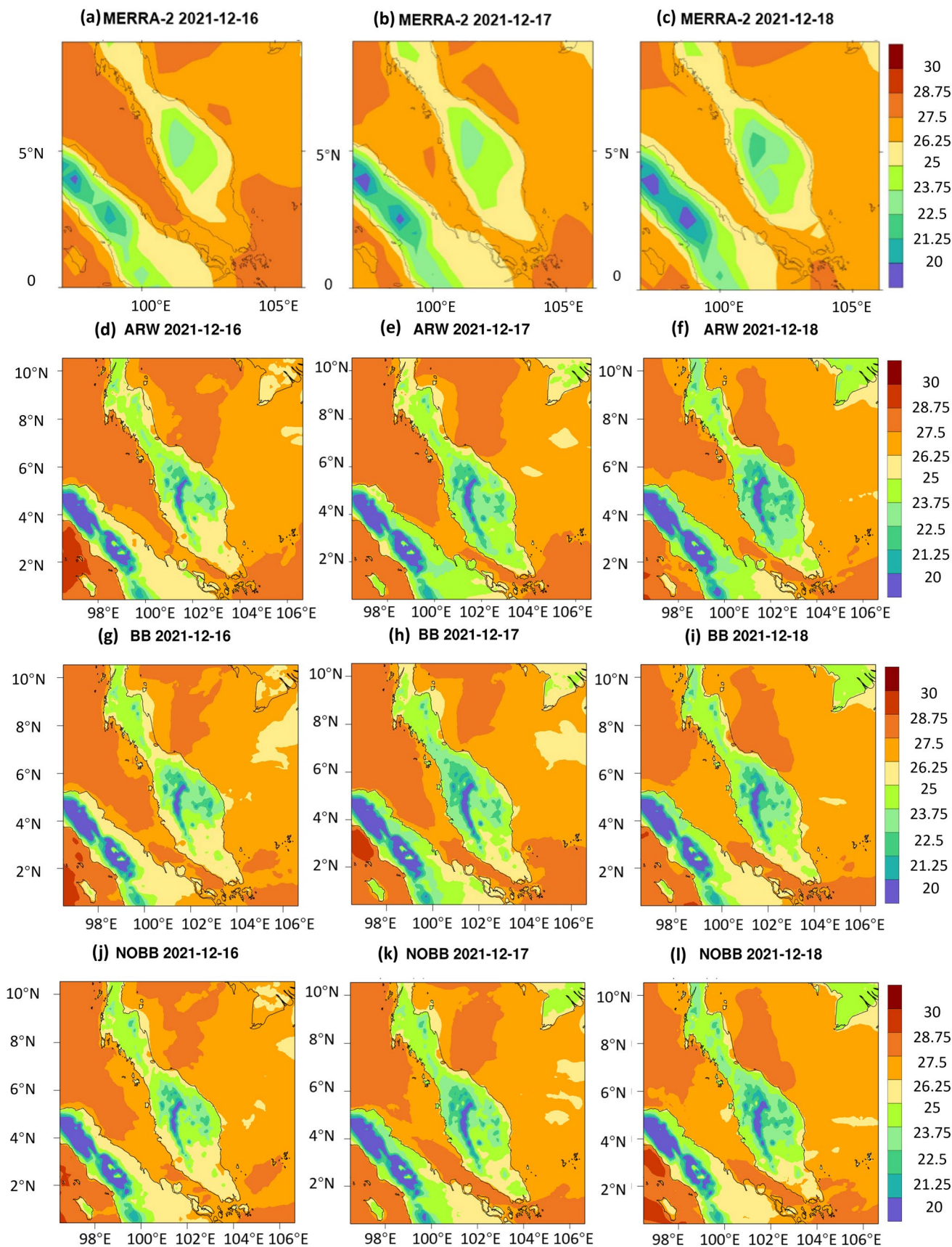
Fig. 16 Spatial distribution of 2-m temperature (°C) from MERRA-2 (**a**, **b**, **c**) against ARW (**d**, **e**, **f**), BB (**g**, **h**, **i**), and NOBB (**j**, **k**, **l**)
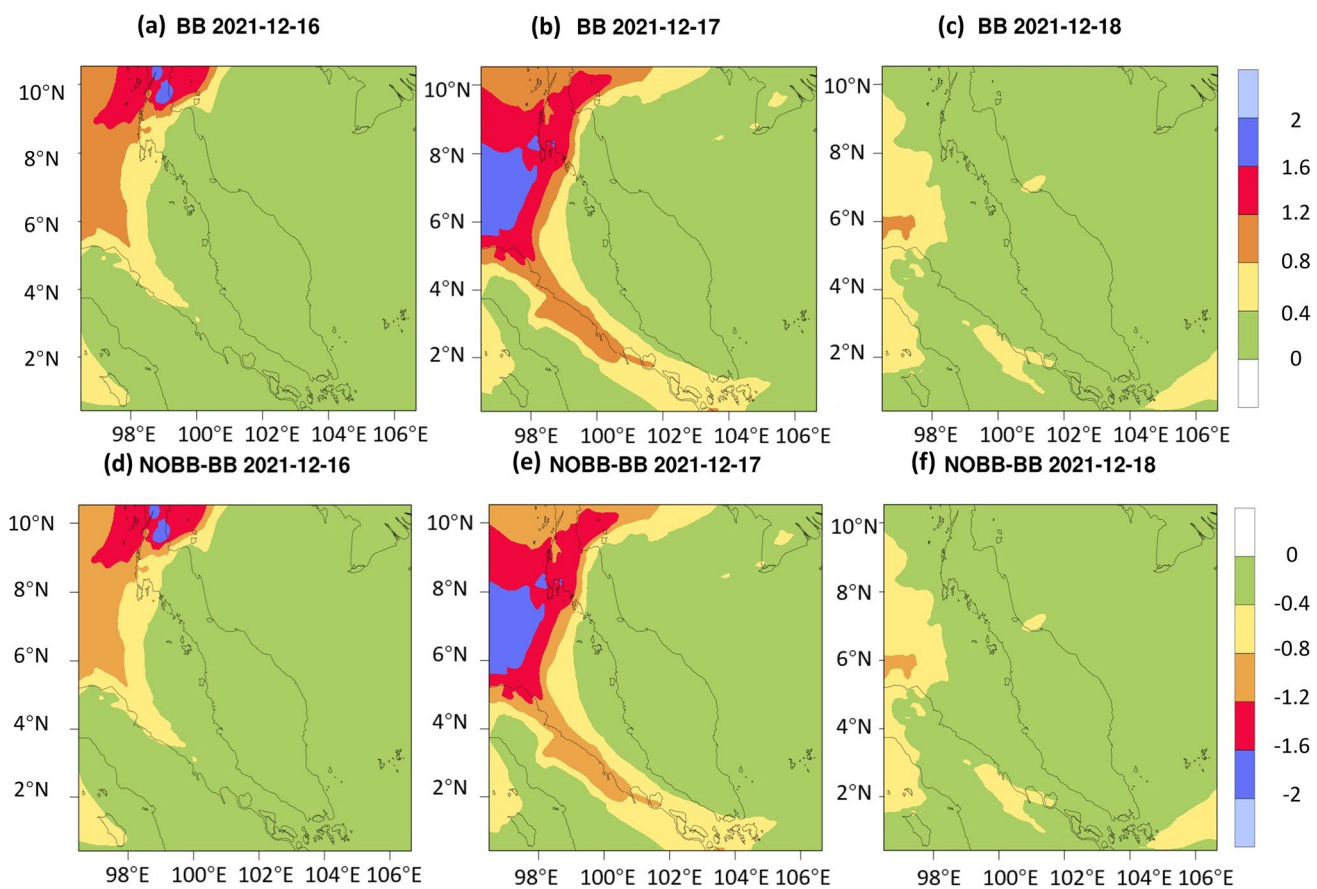
Fig. 17 Spatial distribution of PM$_{2.5}$ concentration in BB (**a**, **b**, **c**) and difference between NOBB and BB (**d**, **e**, **f**) (µg m^{-3}) over PM from 16th to 18th December 2021

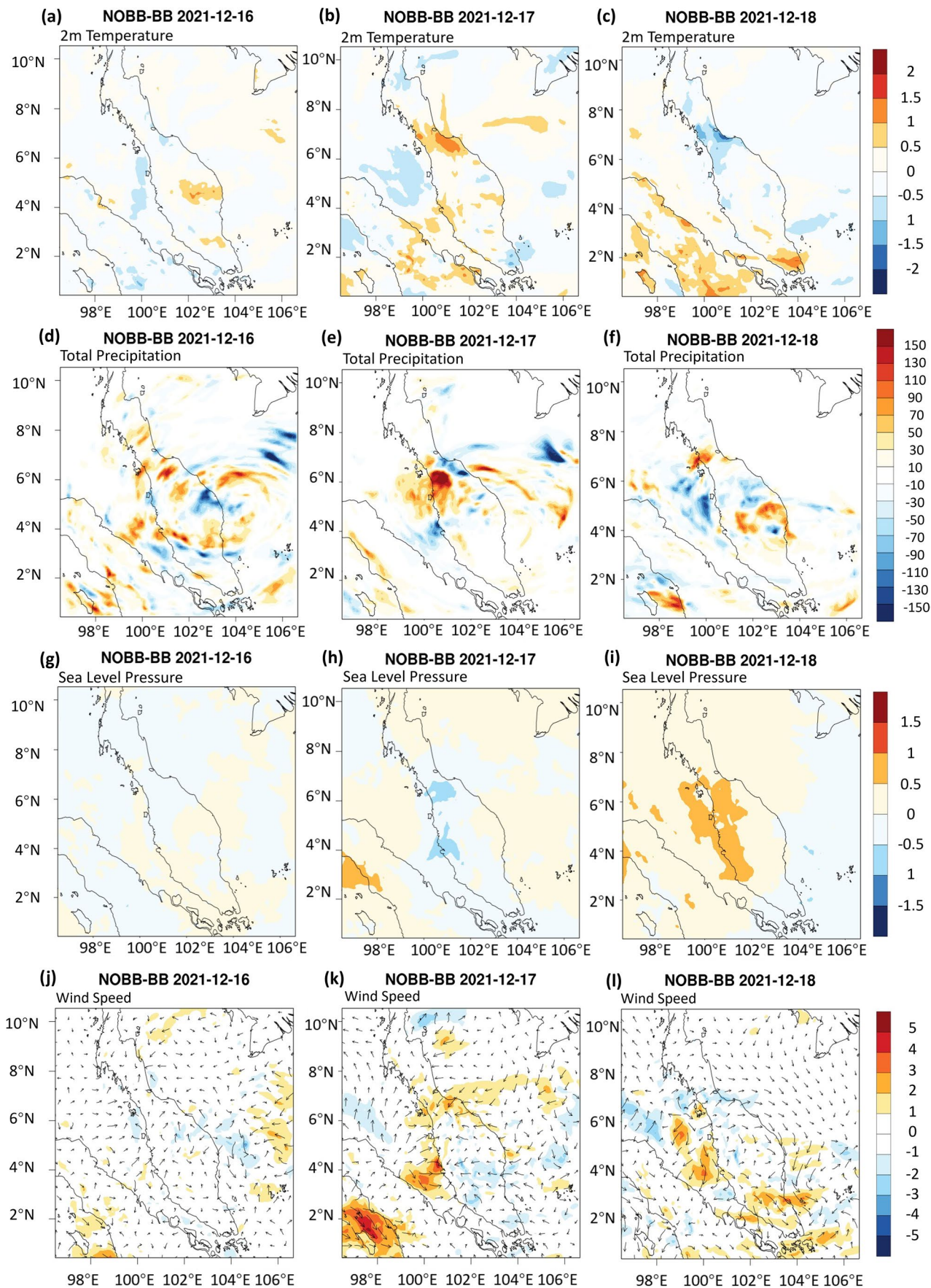**Fig. 18** Spatial distribution of meteorological variables between NOBB and BB. Red (blue) indicate value in NOBB is higher (lower) than BB

Fig. 19 Averaged precipitation of stations over west coast and east coast simulated by BB and NOBB
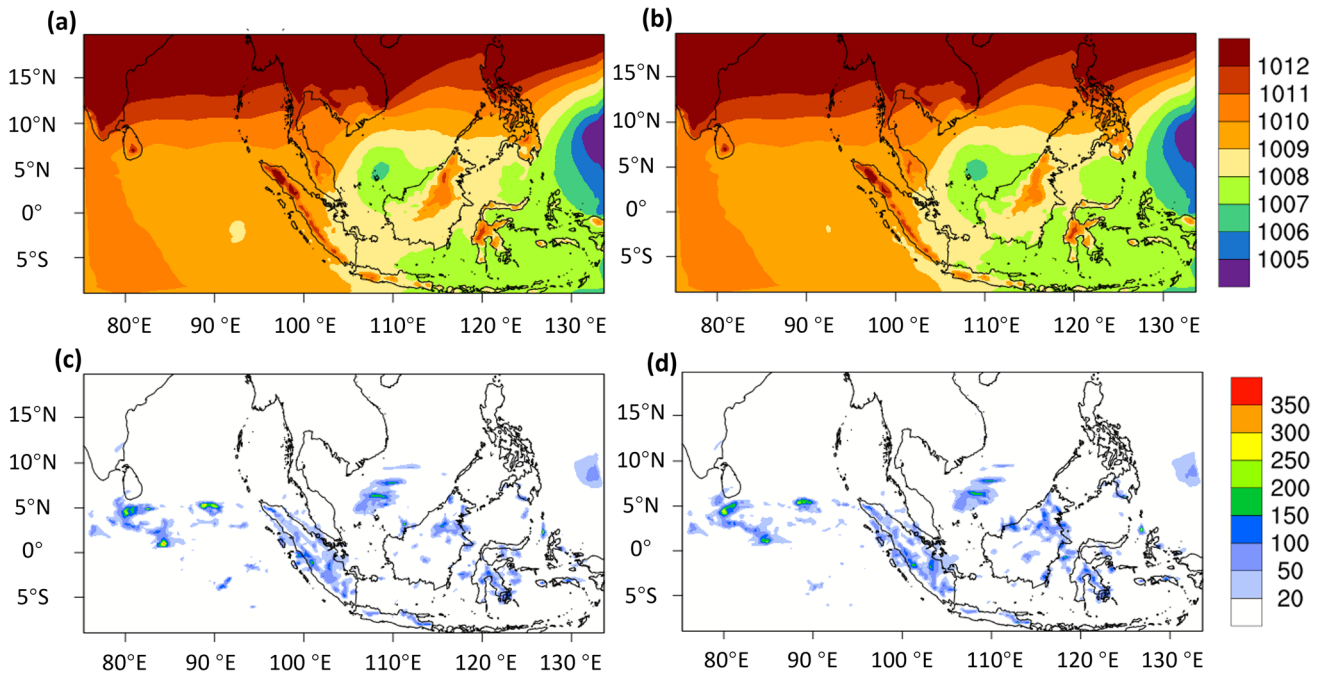
Fig. 20 Spatial distribution of SLP (hPa) and precipitation (mm) on 14th December 2021 in ARW (**a**, **c**) and BB (**b**, **d**)
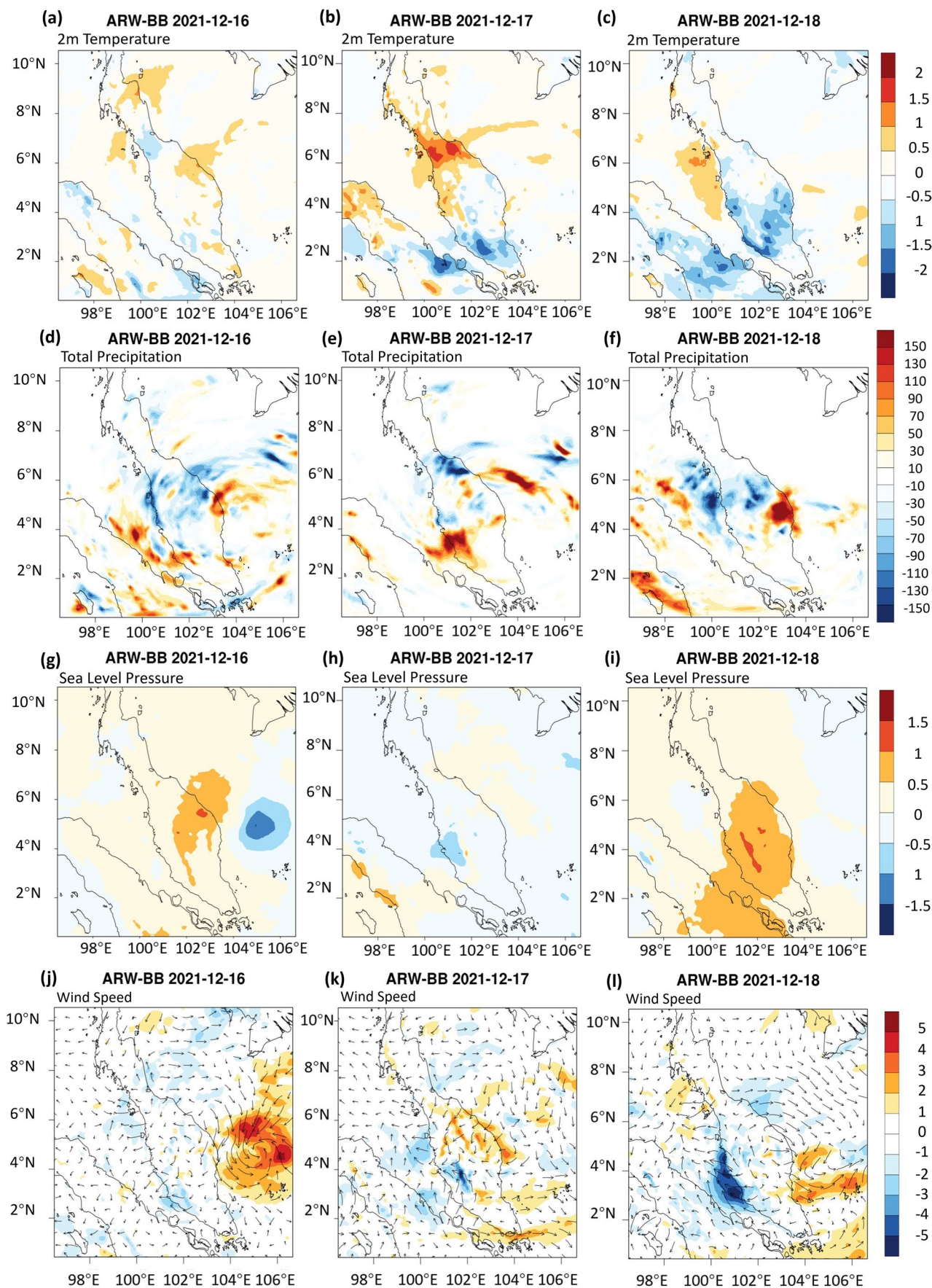
Fig. 21 Spatial distribution of meteorological variables between ARW and BB. Red (blue) indicates value in ARW is higher (lower) than BB

Conclusions

A case of extreme monsoonal flood event affected the East and West coast of Peninsular Malaysia (PM) in December 2021 and brought huge socio-economic damage to the society. In order to study the event, the meteorological characteristics over PM during the study period of 16th to 18th December are investigated. IBTrACS shows the Tropical Depression 29 (TD) was formed and moving from East coast to West coast during the study period. The heavy rainfall area is consistent with the movement of TD center with maximum intensity of 250 mm/day and 300 mm/day over Pahang on 16th December and Selangor during 17th to 18th December respectively. Typhoon Rai does not intensify the rainfall event in the way of transporting moisture to PM as moisture flux divergence between Typhoon Rai and TD is not strong enough.

In order to study the monsoon-driven extreme rainfall event, WRF model is used to reproduce the meteorological variables during the study period with two nests (horizontal resolution of 30 km and 10 km). Most studies from literature use WRF-ARW model with specified gas and aerosol concentration for pure meteorological studies, and WRF-Chem model for air quality simulations as they believe it would provide better performance with predicted gas and aerosol concentration and involvement of chemistry process. While rarely, the study compares the performance between these two models. As biomass burning (BB) aerosols which appears as an annual phenomenon over Southeast Asian also capable on intensifying the rainfall intensity, the effect of BB aerosol on the precipitation also be examined by conduct the model simulation including and excluding the BB emission. Therefore, the model evaluation is carried out for this extreme rainfall event to assess the performance of ARW (WRF-ARW), BB (WRF-Chem with biomass burning), and NOBB (WRF-Chem without biomass burning) in this study. A sensitivity analysis of PBL scheme on WRF-ARW was also conducted, which shows QNSE as the best scheme and used for further assessment.

The result indicates that AWR shows an overall better performance for most meteorological variables. ARW has better performance in reproducing SLP and wind speed with *r* of 0.54 and 0.5 respectively. Model scenario of AWR and BB produce similar TD spatial distributions but differ in the magnitude where TD in ARW is stronger during the study period over East coastline. All models overestimate the precipitation intensity, but ARW was more correlated with observation data followed by NOBB and BB. ARW successfully simulates the heavy rainfall over West coast region on 17th and 16th December while in weaker intensity. Biomass burning aerosols have only a minor effect on intensifying or delaying the rainfall. More attention needs to focus on the low-pressure system for preventing the flooding due to heavy rainfall event during Northeast monsoon season than BB haze event as TD over PM was considered to be the main contributor to the extreme rainfall event.

References

Ahmed M, Guo X, Zhao X-M (2016) Determination and analysis of trace metals and surfactant in air particulate matter during biomass burning haze episode in Malaysia. Atmos Environ 141:219–229

Ajoku O, Norris JR, Miller AJ (2019) Observed monsoon precipitation suppression caused by anomalous interhemispheric aerosol transport. Climate Dynam 54(1-2):1077–1091

Andreae MO, Rosenfeld D, Artaxo P, Costa AA, Frank GP, Longo KM, Silva-Dias MAF (2004) Smoking rain clouds over the Amazon. Science 303:1337–1341

Aouizerats B, van der Werf GR, Balasubramanian R, Betha R (2015) Importance of transboundary transport of biomass burning emis-sions to regional air quality in Southeast Asia during a high fire event. Atmos Chem Phys 15(1):363–373

Avolio E, Federico S, Miglietta MM, Feudo TL, Calidonna CR, Sem-previvA AM (2017) Sensitivity analysis of WRF model PBL schemes in simulating boundary layer variables in southern Italy: An experimental campaign. Atmos Res 192:58–71

Bollasina MA, Ming Y, Ramaswamy V (2011) Anthropogenic aerosols and the weakening of the South Asian summer monsoon. Science 334(6055):502–505

Bosart LF, Carr FH (1978) A case study of excessive rainfall centered around Wellsville, New York, 20–21 June 1972. Mon Weather Rev 106(3):348–362

Caddis B, Nielsen C, Hong W, Anun Tahir P, Yenn Teo F (2012) Guidelines for floodplain development – a Malaysian case study. Int J River Basin Manag 10(2):161–170

Chang C-P, Wang Z, Ju J, Li T (2004) On the relationship between western maritime continent monsoon rainfall and ENSO during northern winter. J Clim 17:665–672

Chang JH-W, Kong SSK, Sentian J, Dayou J, Chee F-P (2019) Synoptic analysis and mesoscale numerical modelling of heavy precipita-tion: a case study of flash flood event in Kota Kinabalu, Malaysia. Meteorol Atmos Phys 132(2):181–201

Cheah R, Billa L, Chan A, Teo FY, Pradhan B, Alamri AM (2019) Geospatial modelling of watershed peak flood discharge in Selangor, Malaysia. Water 11. https://doi.org/10.3390/w11122490

Chen D, Xie X,Zhou Y, Lang J, Xu T, Yang N, Zhao Y, Liu X (2017) Performance evaluation of the WRF-Chem model with different physical parameterization schemes during an extremely high# PM2.5 pollution episode in Beijing. Aerosol Air Qual Res 17(1):262–277

Chen T-C, Wu C-C (2016) The remote effect of Typhoon Megi (2010) on the heavy rainfall over northeastern Taiwan. Mon Weather Rev 144(9):3109–3131

Chen Y, Chan A, Yenn T, Ooi C, Li L (2023) A study of the effect of open biomass burning aerosol on rainfall event over Malaysia by using EOF analysis. IOP Conference Series. Earth Environ Sci 1167(1):12006

Chong XY, Vericat D, Batalla RJ, Teo FY, Lee KSP, Gibbins C (2021) A review of the impacts of dams on the hydromorphology of tropical rivers. Sci Total Environ 794:148686

Crippa, M., Guizzardi, D., Muntean, M. and Schaaf, E. (2021). EDGAR v5.0 global air pollutant emissions, European Commission.

Crippa P, Sullivan RC, Thota A, Pryor SC (2017) The impact of resolution on meteorological, chemical and aerosol properties in regional simulations with WRF-Chem. Atmos Chem Phys 17(2):1511–1528

Fan J, Yuan T, Comstock JM, Ghan S, Khain A, Leung LR, Li Z, Martins VJ, Ovchinnikov M (2009) Dominant role by vertical wind shear in regulating aerosol effects on deep convective clouds. J Geophys Res 114:D22206

Forster, P., V. Ramaswamy, P. Artaxo, T. Berntsen, R. Betts, D.W. Fahey, J. Haywood, J. Lean, D.C. Lowe, G. Myhre, J. Nganga, R. Prinn, G. Raga, M. Schulz and R. Van Dorland (2007). Changes in atmospheric constituents and in radiative forcing. In: Climate Change 2007: The physical science basis. Contribution of Working Group I to the Fourth Assessment Report of the Intergovernmental Panel on Climate Change [Solomon, S., D. Qin, M. Manning, Z. Chen, M. Marquis, K.B. Averyt, M.Tignor and H.L. Miller (eds.)]. Cambridge University Press, Cambridge, United Kingdom and New York, NY, USA

Fung KF, Chew KS, Huang YF, Ahmed AN, Teo FY, Ng JL, Elshafie A (2022) Evaluation of spatial interpolation methods and spatiotemporal modeling of rainfall distribution in Peninsular Malaysia. Ain Shams Eng J 13(2):101571

Global Modeling and Assimilation Office (GMAO) (2015), MERRA-2 tavg1_2d_slv_Nx: 2d,1-hourly, time-averaged, single-level, assimilation, single-level diagnostics V5.12.4, Greenbelt, MD, USA, Goddard Earth Sciences Data and Information Services Center (GES DISC), Accessed: [20 March 2022], 10.5067/VJAFPLI1CSIV.

Grell GA, Peckham SE, Schmitz R, McKeen SA, Frost G, Skamarock WC, Eder B (2005) Fully coupled "online" chemistry within the WRF model. Atmos Environ 39(37):6957–6975

Guenther A (2006) Estimates of global terrestrial isoprene emissions using MEGAN (Model of Emissions of Gases and Aerosols from Nature). Atmos Chem Phys 6:3181–3210

IPCC (2014): Climate change 2014: synthesis report. Contribution of Working Groups I, II and III to the Fifth Assessment Report of the Intergovernmental Panel on Climate Change [Core Writing Team, R.K. Pachauri and L.A. Meyer (eds.)]. IPCC, Geneva, Switzerland, 151 pp.

Islam M, Chan A, Ashfold M, Ooi C, Azari M (2018) Effects of El-Niño, Indian Ocean dipole, and Madden-Julian oscillation on surface air temperature and rainfall anomalies over Southeast Asia in 2015. Atmosphere 9(9):352

Jacobson MZ, Kaufman YJ (2006) Wind reduction by aerosol particles. Geophys Res Lett 33:L24814

Jangid M, Mishra A, Koren I, Sarangi C, Kumar K, Singh S, Tripathi S (2021) Observation of aerosol induced 'lower tropospheric cooling' over Indian core monsoon region. Environ Res Lett 16(12):124057

Janjić Z (1990) The step-mountain coordinate: physical package. Mon Weather Rev 118(7):1429

Janjic Z (2001) Nonsingular implementation of the Mellor-Yamada level 2.5 scheme in the NCEP Meso model. NCEP Office Note 437

Khain A, Pokrovsky A, Pinsky M, Seifert A, Phillips V (2004) Simulation of effects of atmospheric aerosols on deep turbulent convective clouds using a spectral microphysics mixed-phase cumulus Cloud model. Part I: Model description and possible applications. J Atmos Sci 61(24):2963–2982

Koren I, Martins JV, Remer LA, Afargan H (2008) Smoke invigoration versus inhibition of clouds over the Amazon. Science 321:946–949

Lee H-H, Iraqui O, Gu Y, Yim SH-L, Chulakadabba A, Tonks AY-M, Yang Z, Wang C (2018) Impacts of air pollutants from fire and non-fire emissions on the regional air quality in Southeast Asia. Atmos Chem Phys 18(9):6141–6156

Lee H-H, Wang C (2020) The impacts of biomass burning activities on convective systems over the Maritime Continent. Atmos Chem Phys 20(4):2533–2548

Li Z, Lau WKM, Ramanathan V, Wu G, Ding Y, Manoj MG, Liu J, Qian Y, Li J, Zhou T, Fan J, Rosenfeld D, Ming Y, Wang Y, Huang J, Wang B, Xu X, Lee SS, Cribb M et al (2016) Aerosol and monsoon climate interactions over Asia. Rev Geophys 54(4):866–929

Lim SY, Marzin C, Xavier P, Chang C-P, Timbal B (2017) Impacts of boreal winter monsoon cold surges and the interaction with MJO on Southeast Asia rainfall. J Climate 30(11):4267–4281

Lin Y-H, Wu C-C (2021) Remote rainfall of Typhoon Khanun (2017): monsoon mode and topographic mode. Mon Weather Rev 149(3):733–752

Liu C, Huang J, Hu XM, Hu C, Wang Y, Fang X, Luo L, Xiao HW, Xiao HY (2021) Evaluation of WRF-Chem simulations on vertical profiles of PM2.5 with UAV observations during a haze pollution event. Atmos Environ 252(1994):118332

Loo YY, Billa L, Singh A (2015) Effect of climate change on seasonal monsoon in Asia and its impact on the variability of monsoon rainfall in Southeast Asia. Geosci Front 6(6):817–823

Moya-álvarez A, Gálvez J, Holguín A, Estevan R, Kumar S, Villalobos E, Silva Y (2018) Extreme rainfall forecast with the WRF-ARW model in the Central Andes of Peru. Atmosphere 9(9):362

Myhre, G., D. Shindell, F.-M. Bréon, W. Collins, J. Fuglestvedt, J. Huang, D. Koch, J.-F. Lamarque, D. Lee, B. Mendoza, T. Nakajima, A. Robock, G. Stephens, T. Takemura and H. Zhang (2013). Anthropogenic and natural radiative forcing. In: Climate change 2013: the physical science basis. Contribution of Working Group I to the Fifth Assessment Report of the Intergovernmental Panel on Climate Change [Stocker, T.F., D. Qin, G.-K. Plattner, M. Tignor, S.K. Allen, J. Boschung, A. Nauels, Y. Xia, V. Bex and P.M. Midgley (eds.)]. Cambridge University Press, Cambridge, United Kingdom and New York, NY, USA, pp. 659–740

National Centers for Environmental Prediction/National Weather Service/NOAA/U.S. Department of Commerce (2004) NCEP ADP Global Surface Observational Weather Data, October 1999 - continuing (Updated daily) [Dataset]. Research Data Archive at the National Center for Atmospheric Research, Computational and Information Systems Laboratory. https://doi.org/10.5065/4F4P-E398 Accessed 26 April. 2022

Oozeer MY, Chan A, Ooi MC-G, Zarzur AM, Salinas SV, Chew B-N, Morris KI, Choong W-K (2016) Numerical study of the transport and convective mechanisms of biomass burning haze in South-Southeast Asia. Aerosol Air Qual Res 16(11):2950–2963

Pegahfar N, Gharaylou M, Shoushtari MH (2022) Assessing the performance of the WRF model cumulus parameterization schemes for the simulation of five heavy rainfall events over the Pol-Dokhtar, Iran during 1999–2019. Springer 112:253–279

Pleim J (2007) A combined local and nonlocal closure model for the atmospheric boundary layer. Part I: model description and testing. J Appl Meteorol Climatol 46:1383–1395

Rahman S (2022) Malaysia's floods of December 2021: can future disasters be avoided? Researchers at ISEAS–Yusof Ishak Institute analyse current events. ISEAS–Yusof Ishak Institute, Singapore

Rai D, Pattnaik S (2019) Evaluation of WRF planetary boundary layer parameterization schemes for simulation of monsoon depressions over India. Meteorol Atmos Phys 131(5):1529–1548

Rosenfeld D, Lohmann U, Raga GB, O'Dowd CD, Kulmala M, Fuzzi S, Reissell A, Andreae MO (2008) Flood or drought: How do aerosols affect precipitation? Science 321:1309–1313

Sani GDI, Muhd B, Mohd E, Musa GA (2014) Floods in Malaysia: historical review, causes, effect and mitigation approach. Int J Interdisciplinary Res Innov 2(4):59–65

Schwartz SE (1996) The whitehouse effect: shortwave radiative forcing of climate by anthropogenic aerosols: an overview. J Aerosol Sci 27:359–382

Stensrud, D. J. (2007). Parameterization schemes: keys to understanding numerical weather prediction models. Cambridge University Press: 459.

Sukoriansky S, Galperin B, Perov V (2005) Application of a new spectral theory of stably stratified turbulence to atmospheric boundary layers over sea ice. BoundaryLayer Meteorol 117(2):231–257

Tan ML, Santo H (2018) Comparison of GPM IMERG, TMPA 3B42 and PERSIANN-CDR satellite precipitation products over Malaysia. Atmos Res 202:63–76

Tan WY, Lai SH, Teo FY, Armaghani DJ, Pavitra K, El-Shafie A (2022) Three steps towards better forecasting for streamflow deep learning. Appl Sci 12:12567

Tao W, Li X, Khain A, Matsui T, Lang S, Simpson J (2007) Role of atmospheric aerosol concentration on deep convective precipitation: cloud-resolving model simulations. Journal of Geophysical Research 112(D24):D24S18-N/a

Tew YL, Tan ML, Juneng L, Chun KP, Hassan MHB, Osman SB, Samat N, Chang CK, Kabir MH (2022) Rapid Extreme tropical precipitation and flood inundation mapping framework (RETRACE): initial testing for the 2021–2022 Malaysia flood. ISPRS Int J Geo Inf 11(7):378

Tomasi E, Giovannini L, Zardi D, de Franceschi M (2017) Optimization of Noah and Noah_MP WRF land surface schemes in snow-melting conditions over complex terrain. Mon. Wea. Rev 145:4727–4745

Tsay J-D, Chen T-C, Yen M-C, Matsumoto J (2013) Interannual variation of the winter rainfall in Malaysia caused by the activity of rain-producing disturbances. J Climate 26(13):4630–4648

Twomey (1997) The influence of pollution on the shortwave albedo of clouds. J Atmos Sci 34:1149–1152

Valappil V, Kedia S, Dwivedi A, Pokale S, Islam S, Khare M (2023) Assessing the performance of WRF ARW model in simulating heavy rainfall events over the Pune region: In support of operational applications. Meteorol Atmos Phys 135(2):16

Verma S, Panda J, Rath S (2021) Role of PBL and microphysical parameterizations during WRF simulated monsoonal heavy rainfall episodes over Mumbai. Pure Appl Geophys 178(9):3673–3702

Wang Y, Wang Y, Fudeyasu H (2009) The role of Typhoon Songda (2004) in producing distantly located heavy rainfall in Japan*. Mon Weather Rev 137(11):3699–3716

Wiedinmyer C, Akagi SK, Yokelson RJ, Emmons LK, Al-Saadi JA, Orlando JJ, Soja AJ (2011) The Fire INventory from NCAR (FINN): a high resolution global model to estimate the emissions from open burning. Geosci Model Dev 4(3):625–641

Wu G, Li Z, Fu C, Zhang X, Zhang R, Zhang R, Zhou T, Li J, Li J, Zhou D, Wu L, Zhou L, He B, Huang R (2015) Advances in studying interactions between aerosols and monsoon in China. Sci China Earth Sci 59(1):1–16

Xia J, Teo FY, Falconer RA, Qian C, Deng S (2016) Hydrodynamic experiments on the impacts of vehicle blockages at bridges. J Flood Risk Manage 11:S395–S402

Yahya K, Wang K, Campbell P, Chen Y, Glotfelty T, He J, Pirhalla M, Zhang Y (2017) Decadal application of WRF/Chem for regional air quality and climate modeling over the U.S. under the representative concentration pathways scenarios. Part 1: model evaluation and impact of downscaling. Atmos Environ 152:562–583

Yahya K, Wang K, Campbell P, Glotfelty T, He J, Zhang Y (2016) Decadal evaluation of regional climate, air quality, and their interactions over the continental US and their interactions using WRF/Chem version 3.6.1. Geosci Model Dev 9(2):671–695

Zaveri RA, Easter RC, Fast JD, Peters LK (2008) Model for simulating aerosol interactions and chemistry (MOSAIC). J. Geophys Res 113:D13204

Zhao C, Yang Y, Fan H, Huang J, Fu Y, Zhang X, Kang S, Cong Z, Letu H, Menenti M (2020) Aerosol characteristics and impacts on weather and climate over the Tibetan Plateau. Natl Sci Rev 7:492–495

Zhou Y, Han Z, Liu R, Zhu B, Li J, Zhang R (2018) A modeling study of the impact of crop residue burning on PM2.5 concentration in Beijing and Tianjin during a severe autumn haze event. Aerosol Air Qual Res 18(7):1558–1572